UNIVERSITY OF OKLAHOMA

GRADUATE COLLEGE

SUBSURFACE PRESSURE MODELING OF SALTWATER DISPOSAL FOR THE ARBUCKLE AND TIMBERED HILLS-BASEMENT SYSTEM, ANADARKO SHELF, OKLAHOMA

A THESIS

SUBMITTED TO THE GRADUATE FACULTY

in partial fulfillment of the requirements for the

Degree of

MASTER OF SCIENCE

By

MARLENA RUTH MCCONVILLE
Norman, Oklahoma
2018

Downloaded from SHAREOK. Persistent Handle URL: https://hdl.handle.net/11244/301991

SUBSURFACE PRESSURE MODELING OF SALTWATER DISPOSAL FOR THE ARBUCKLE AND TIMBERED HILLS-BASEMENT SYSTEM, ANADARKO SHELF, OKLAHOMA

A THESIS APPROVED FOR THE
CONOCOPHILLIPS SCHOOL OF GEOLOGY AND GEOPHYSICS

BY

Dr. R. Douglas Elmore, Co-Chair

Dr. Kyle E. Murray, Co-Chair

Dr. Matthew J. Pranter

© Copyright by MARLENA RUTH MCCONVILLE 2018
All Rights Reserved.

Table of Contents

List of Tables vi

List of Figures viii

Abstract xii

Chapter 1: Introduction 1

Chapter 2: Previous Studies 2

Chapter 3: Geologic Setting 5

Chapter 4: Current Study 8

4.1 Study Area 8

4.2 Injection History 9

4.3 Downhole Pressure Monitoring 10

4.6 Research Objectives 12

Chapter 5: Methodology 12

5.1 Build Conceptual Model 12

5.1.1 Define Model Layers 13

5.1.2 Define Layer Properties 14

5.1.3 Compile Arbuckle Group Data 16

5.1.4 Identify Arbuckle Facies 19

5.1.5 Define Layer Pressure/Hydraulic Head 20

5.1.6 Identify Geologic Structures 22

5.2 Numerical Model 23

5.3 Setup Steady-State Model 24

5.3.1 Model Domain 24

5.3.2 Boundary Conditions 25
5.3.3 Input Parameters 26
5.4 Setup Transient Model 28
5.4.1 Specific Storage 29
5.4.2 Monitoring Well Data 31
5.4.3 Model Assumptions 32
Chapter 6: Results 33
6.2 Steady-State Model Results 33
6.3 Transient Model Results 36
6.3.1 Scenario 1: Arbuckle Sub-layers 41
6.3.2 Scenario 2: Faults with uniform properties 44
6.3.4 Scenario 3: Varying fault properties 49
6.3.5 Inferred Faults 49
6.4 Evaluation of Model Calibration/Measures of Error 52
Chapter 7: Discussion 59
Chapter 8: Conclusions and Future Work 62
8.1 Conclusions 62
8.2 Future Work 66
References 67
Appendix A: Sensitivity Analysis Plots for Transient Model 74

List of Tables

Table 1: Chronostratigraphic and lithostratigraphic chart of the basement rock, Arbuckle Group, and Simpson Group of Oklahoma (modified from Christenson et al., 2011). 7

Table 2: Geographic locations and API numbers of the six pressure-monitoring wells located within the study area/model domain. 12

Table 3: Disposal water properties from the U.S. Geological Survey National Produced Waters Geochemical Database (Blondes et al., 2017; and Dessouky and Ettouney, 2002). 15

Table 4: Arbuckle properties derived from earth tide analysis of pressure monitoring data (Perilla, 2017). 18

Table 5: Summary of model inputs and initial parameters for the model based on previous studies (Puckette, 1996; Carrell, 2014; and Perilla, 2017). 27

Table 6: Observation points representing the locations of the Fairview mainshock, foreshocks, and additional locations/depths of interest. Simulated pressure at these locations will be evaluated and compared to seismic events in the Fairview sequence. 30

Table 7: Initial head pressure values (m) at each monitoring well (Puckette, 1996)..... 32

Table 8: Resulting table of sensitivity analysis for steady-state model. Correlation coefficient is measured to compare simulated hydraulic head values for the Arbuckle Group to initial conditions from Puckette, 1996. 34

Table 9: Best fit hydraulic properties obtained from steady-state model calibration used for initial parameters of the transient model. 36

Table 10: Model parameters used for the Scenario 1 of the various scenarios used to simulate the transient model. 41

Table 11: Model parameters used for transient model to run Scenario 2 and observe head changes within monitoring wells. 45
Table 12: Initial parameters used for Scenario 3 of the transient model simulations. 49
Table 13: Initial heads for each of the monitoring wells from Puckette (1996) used to calibrate the steady-state model compared to observed values from April 2018 and simulated values for April 2018. 63

List of Figures

Figure 1: Study area in north-central Oklahoma. Cataloged faults from Oklahoma Geological Survey fault database (Marsh and Holland, 2016)..... 8

Figure 2: Cumulative injection volumes for saltwater disposal wells in model domain (Fairview region). 10

Figure 3: Pressure monitoring wells instrumented by the OGS in the Monitoring and Analysis of Arbuckle Group Pressures project. Fifteen wells are instrumented and continuously measuring pressure and temperature every 30 seconds. 11

Figure 4: Model layers defined in ModelMuse with elevation of the model about 400 m and bottom depth of the four-layer model at -9000 m. 13

Figure 5: Potentiometric surface map of Oklahoma compiled by Puckette (1996). The hydraulic head values are used as the initial conditions for steady-state modeling. 21

Figure 6: Model domain for the numerical simulations using MODFLOW (Harbaugh, 2005). Model area dimensions include 54 km x 90 km area (4860 km²) including 113 SWD wells, six monitoring wells, and faults from Oklahoma Geological Survey Fault database (Marsh and Holland, 2016). Initial head contours (m) from Puckette (1996). 22

Figure 7: Model domain discretized for the numerical simulations using MODFLOW (Harbaugh, 2005). Model area dimensions include 54 km x 90 km (4860 km²) and each cell is 1 km². 25

Figure 8: ModelMuse image of the model domain for transient model simulations. The observation points (Table 6) to compute pressure changes within the Arbuckle and Timbered Hills-Basement are highlighted in yellow..... 31

Figure 9: Assigned model parameters for initial steady state model against the initial hydraulic head values from Puckette, 1996 35

Figure 10: Observed vs simulated values for the initial parameters for the transient model acquired from the calibrated steady state model..... 36
Figure 11: Pressure results for Alfalfa_01 and Alfalfa_04 from the sensitivity analysis performed on the transient model by varying parameters of the Arbuckle and Timbered Hills-Basement layer..... 37
Figure 12: Pressure results for Grant_05 and Grant_06 from the sensitivity analysis performed on the transient model by varying parameters of the Arbuckle and Timbered Hills-Basement layer. 38
Figure 13: Pressure change computed at observation point, Fairview 2, located at a depth of 4.05 km. Pressure changes for the transient sensitivity analysis are simulated from January 2009–June 2017..... 39
Figure 14: Pressure change at observation point, Observation 1, located about 4 km from Alfalfa_04 and Grant_05 at a depth of 4 km. 40
Figure 15: Simulating the resulting hydraulic head values of Alfalfa_01 and Grant_06 with uniform hydraulic conductivity values for all three sub-layers (Upper, Middle, and Lower)..... 42
Figure 16: Results of Scenario 2 varying the conductivity of each of three sub-layers of the Arbuckle layer. The top plot shows hydraulic head results of an impermeable Upper and Lower Sub-layer. The bottom diagram shows the results of a less impermeable Middle Sub-layer..... 43
Figure 17: Top diagram shows pressure changes in Alfalfa_01 with the presence of faults. The bottom plot shows previously mapped faults within the model domain with uniform permeability at different elevations..... 46
Figure 18: Results of Scenario 2 for the transient model and the head values simulated in Alfalfa_04. 47

Figure 19: Results of uniform fault permeability at different elevations within the Arbuckle layer for Grant_05 and Grant_06. 48
Figure 20: Map of study area showing shallow earthquakes around Alfalfa_02 and Alfalfa_03 less than 4 km in depth..... 50
Figure 21: A map of the study area produced by Alt and Zoback (2017) to show fault planes (green lines) assumed to have slipped to produce the earthquakes events shown as red dots. These “inferred” faults were mapped using available focal mechanism solutions and stress orientations from wellbore hole data (Alt and Zoback, 2107). The black lines represent previously cataloged faults. 51
Figure 22: ModelMuse image of inferred faults placed in the model domain assigned a hydraulic conductivity of 0.95 m/d. 52
Figure 23: Observed/simulated values and head residuals plotted for the six monitoring wells during calibration (September 2016–July 2017). If there is a perfect match, then head values would be aligned along the dotted line. 53
Figure 24: Change in observed vs simulated head pressure values (m) in Alfalfa_03 and Alfalfa_04 values for final calibrated model. 54
Figure 25: Change in observed vs simulated head pressure values (m) in Grant_05 and Grant_06 values for final calibrated model..... 55
Figure 26: Sensitivity analysis performed on the calibrated transient model. Hydraulic head results for Alfalfa_01 and Grant_06. 56
Figure 27: Calibrated (September 2016–June 2017) and validated (July 2017–April 2018) head values for monitoring wells located in Alfalfa County..... 58

Figure 28: Calibrated (September 2016–June 2017) and validated (July 2017–April 2018) head values for monitoring wells located in Grant County. 59
Figure 29: Observation 2 is an observation point located near the Fairview earthquake sequence. Pressure changes are recorded at 3 km for the entire duration of the model (January 2009–April 2018). 61
Figure 30: Smaller pressure changes are computed at Observation 2 when all faults within the model are permeable. Figure 29 shows pressure changes for the calibrated model which assigns faults as both permeable and impermeable. 62
Figure 31: Potentiometric surface map showing hydraulic heads (m) one month/ time step in the transient simulation (February 2009) and after 112 months /time steps (April 2018)..... 64
Figure 32: Total head change (m) for the Arbuckle and TH-B layer after 112 months/time steps, represented by a color grid and contours. The distance between the largest increase in head change to zero head change is 45 km..... 65

Abstract

Increased saltwater disposal (SWD) into a geologic zone, the Arbuckle Group, has been related to higher than background levels of seismicity in Oklahoma since 2009. Recent studies have shown statistical associations of saltwater disposal rates, and some hydrogeological models have suggested that pressure in the Arbuckle and basement increased after increased SWD rates. However, previous attempts to model the influence of SWD on pressures within the Arbuckle Group and Basement rock of Oklahoma lacked downhole pressure observations to use for calibration and validation. The present study created a four-dimensional (x, y, z, time) hydrogeologic model calibrated against downhole pressure data to better illustrate SWD injection effects on pressure propagation in the Arbuckle Group and its potential contribution to seismicity.

Fifteen inactive Arbuckle SWD wells located in areas of high-rate injection and seismicity, have been instrumented since August 2016 with pressure transducers to collect high-resolution pressure data every 30 seconds. A four-layer groundwater flow model was constructed using Modular Three-Dimensional Finite-Difference Groundwater Flow (MODFLOW) within the Anadarko Shelf region in northwestern Oklahoma encompassing six of the monitoring wells. The model was run under steady-state conditions and transient conditions to simulate pressure propagation from active SWD wells.

A transient MODFLOW model was calibrated against pressure data collected from the instrumented inactive SWD wells. Previously published hydraulic conductivity and specific storage must be increased by one to two orders of magnitude to match simulated to observed heads using the MODFLOW model. The best fit hydraulic conductivity and specific storage values are 1.9 m/d and 4.53E-07 m^{-1}, respectively. Previous studies suggest a heterogenous and

anisotropic Arbuckle Group, so this study assigns the Middle Sub-layer of the Arbuckle as less permeable than the Upper and Lower Sub-layers, decreasing the head residual in Grant_06, but increasing the residual in Alfalfa wells. With the Arbuckle as a homogenous and isotropic unit, a fault zone of higher vertical conductivity that emulates vertical anisotropy must be present near Alfalfa_02 and Alfalfa_03 to fit simulated heads to observed heads. Using the calibrated groundwater flow model, there was not a significant simulated pressure change in the Timbered Hills-Basement near the location of the Fairview earthquake sequence.

Chapter 1: Introduction

Scientific consensus links increased seismicity in Oklahoma to high injection rates into Class II Underground Injection Control (UIC) saltwater disposal (SWD) wells (Ellsworth, 2013; and National Research Council, 2013). In Oklahoma, the Arbuckle Group receives over 50% of SWD volumes (Murray, 2015). The top of the Arbuckle Group (i.e., Arbuckle) is 3048 m (10000 ft) to 3962 m (13000 ft) below the surface in north-central Oklahoma (Crain and Chang, 2018). From 2009 to 2017, the OGS Earthquake Catalogs show the mean depth for Oklahoma earthquakes as 5151 m (16400 ft) (http://www.ou.edu/ogs/research/earthquakes/catalogs).

An earthquake can be triggered by fluid pore pressure reducing the effective stress and stability of a fault, which results in failure under the prevailing regional stress field (Walsh and Zoback, 2015). Additionally, in the saturated reservoir, increased pressure from SWD can expand or contract the rock matrix, referred to as elasticity (Fetter, 2001). Although poroelastic effects play a role in injection-induced seismicity, pore-pressure diffusion is considered the main contributor (Barbour et al., 2017). Previous hydrogeological studies modeling wastewater disposal into the Arbuckle Group analyze statistical relationships between disposal well location, injection volumes, and earthquake hypocenters to explore the spatiotemporal relationship between SWD and seismicity in Oklahoma (Keranen et al., 2014; Walsh and Zoback, 2015; Weingarten et al., 2015; Weingarten, 2016; Goebel et al., 2016; and Goebel et al., 2017). Current studies use seismological methods to resolve hydrogeological parameters of the Arbuckle, Timbered Hills-Basement, and faults then compute expected pore pressure variations from SWD (Ogwari and Horton, 2016). Previous studies have not had sufficient hydrogeological data to calibrate pore-pressure diffusion, poroelastic, or numerical groundwater flow models of the Arbuckle and Basement complex. This study utilizes site-specific hydrogeological data to better

understand rock properties of the Arbuckle Group in Oklahoma, and to calibrate and validate simulations against field observations.

Chapter 2: Previous Studies

Groundwater flow models have been developed for locations within Oklahoma to investigate wastewater injection into the Arbuckle Group, including the Fairview region (Keranen et al., 2014; Carrell, 2014; and Yeck et al., 2017). Carrell (2014) built a Modular Three-Dimensional Finite-Difference Groundwater Flow Model (MODFLOW) numerical model for the Dilworth Field in north Oklahoma in the Nemaha Uplift geologic province. The model showed that pressure in the Arbuckle substantially increased when simulating SWD wells at 304 m (1000 ft) from a normal fault. The Dilworth Field is identified as a horst/graben structure. Results showed a decrease in hydraulic head of 76 m (250 ft) around production wells within the horst block and an increase in hydraulic head of 67 m (220 ft) within the graben. Consequently, an injection well's radius of influence can be 10 km (6.2 mi) or more (Carrell, 2014). Initial rock properties are gathered from Carrell (2014) because his study site is in northern Oklahoma close to the present study area.

Studies on injection-induced seismicity strive to understand the importance of SWD factors including maximum disposal rate, total volume of disposal, proximity to basement, and distance between SWD well and earthquake epicenters or swarms (Keranen et al., 2014; and Weingarten et al., 2015). Additional site-specific studies in Oklahoma have shown spatiotemporal relationships between injection and seismicity by identifying a region of high-rate injection wells near earthquake activity (Keranen et al., 2013; Keranen et al., 2014; Weingarten et al., 2015; and Barbour et al., 2017). Theories from previous studies conclude that earthquake occurrence and

magnitude are influenced by injection rates of SWD wells (Keranen et al., 2014). Low rate SWD will not necessarily increase the pressure/stress above the “critical threshold” to trigger an earthquake (Keranen et al., 2014).

Keranen et al. (2014) created a hydrogeological model that simulated pressure propagation within the Arbuckle Group up to 48 km (30 mi) from high rate SWD wells to an earthquake swarm near Jones, OK. The model predicted higher fluid pressure perturbation near the wells with higher injection rates. The Jones earthquake swarm occurred after the simulated arrival time of a pressure front within the Arbuckle Group. The results indicated a critical threshold of about 0.07 MPa above which earthquakes are triggered (Keranen et al., 2014). Conclusions from this modeling study showed injection-linked seismicity near Jones occurred up to 34 km (21 mi) away from high -rate SWD wells. The absence of earthquakes in regions above the critical pressure threshold may result from either a lack of faults or lack of optimally-oriented faults.

The Arbuckle Group has a hydrodynamic nature and heterogenous pore-pressure distributions that are indicative of reservoir compartmentalization. Regional variations in pore-pressure from the compartmentalization of the sedimentary section could be caused by faults and other spatial variations in permeability (Keranen et al., 2013; and Barbour et al., 2017). Previous studies state a need for a network of pressure-monitoring wells needed to investigate the reservoir compartmentalization within the Arbuckle Group from stratigraphic and structural features (Barbour et al., 2017). Additional hydrogeological data to study injection-induced seismicity is shown as necessary (Hornbach et al., 2015; and Barnes and Halihan, 2018).

In other hydrogeological models for the Arbuckle Group, specifically in the Fairview region, there has been an effort to couple the poroelastic stress equation with pore-pressure diffusion or groundwater flow equations (Goebel et al., 2017; and Barbour et al., 2017). Injecting water into

a rock matrix increases the hydraulic head; therefore, the effective stress of the aquifer/reservoir decreases and impacts the rock matrix (Goebel et al., 2017). A compressed rock matrix reduces porosity and storage of the aquifer/reservoir. Faults increase the reservoir storativity, which can accommodate more fluid injection or withdrawal before a pore pressure change occurs (Goebel et al., 2017). Fewer changes in pore pressure are observed when faults do not extend from nearby high-rate injection wells to the Fairview earthquakes (only about 0.01 – 0.02 MPa at 3 km), and total expected pressure changes at the distance of Fairview and Woodward seismicity is 0.003–0.100 MPa (3–100 kPa).

Goebel et al. (2017) concludes that pore pressure and elastic stress effects are necessary to trigger faults at such large distances. Depending on the geology and boundary conditions of the area, poroelastic stresses may exceed pore-pressure perturbations at large distances on faults that are not necessarily hydraulically connected (Goebel et al., 2017).

For the current modeling project, the study area includes a section that crosses the Oklahoma- Kansas border. Since 2013, Kansas has also experienced an increase in seismic activity, suspected to be related to dozens of high-rate injection wells near the Oklahoma-Kansas border (Peterie et al., 2018). Pore pressure changes resulting from high-rate SWD wells are believed to induce earthquakes at hypocentral distances of up to 20 km (12 mi) (Keranen et al., 2014; and Yeck et al., 2016). Published studies for Kansas suggest pressure increases, up to 90 km away, that correlate with high-rate injection wells (Peterie et al., 2018).

Chapter 3: Geologic Setting

The oldest rocks in Oklahoma were deposited during the Precambrian and Cambrian, consisting of rhyolites and granites (Johnson, 1991). Hereafter referred to as the Basement, the igneous rocks lie below the Arbuckle Group and the discontinuous Reagan Sandstone, which is part of the Timbered Hills Group. The top of the Basement is about 300 m (1000 ft) below the surface near the Ozark Uplift in northeastern Oklahoma, but is deeper in the basins of Oklahoma, at depths of up to 9144–12192 m (30000–40000 ft) below the ground surface. During the Late Cambrian, Oklahoma experienced inundation and erosion from shallow seas, eroding the basement rocks and depositing the Timbered Hills Group. During the Late Cambrian and Early Ordovician, marine sedimentary dolomite and limestone formations of the Arbuckle Group were deposited on top of the Timbered Hills (Franseen et al., 2004). The Arbuckle Group thickness ranged from 300–600 m (1000–2000 ft) in the Cherokee Platform to 2100 m (7000 ft) in the Southern Oklahoma Aulacogen (Johnson et al., 2008). The Arbuckle is thinner in Kansas, ranging from 60–120 m (200–400 ft) in the northern part of the state (Carr et al., 1986). Peritidal deposition of carbonate sediment, dolomitization, karstification, and numerous fracture-forming events in the Pennsylvanian formed and altered the Arbuckle as a heterogenous reservoir (Fritz et al., 2013).

The Simpson Group, overlying the Arbuckle, contains beds of shale and sandstone that form an impermeable seal over the Arbuckle making it a confined reservoir or aquifer (Carr et al., 1986). This study focuses on the Arbuckle Group as a reservoir for Class II UIC SWD wells. Porosity and permeability of the Arbuckle is controlled by various factors including original depositional material, diagenetic processes, and karstification (Ragland and Donovan, 1991). Core and other logs show collapsed breccias, which indicate that karst and other cavernous

features are likely present within the Arbuckle Group. The Arbuckle and Simpson collectively form the Arbuckle-Simple aquifer, which is a sole source aquifer for parts of south-central Oklahoma. Uplift, subaerial exposure, and erosion of the sediment allowed for a pore network to create a hydrodynamic reservoir found to be underpressured and an excellent repository for SWD (Puckette, 1996).

Time-stratigraphic unit	*Rock-stratigraphic unit*	
Quaternary		Alluvium
Cretaceous		Caddo Limestone Kiamichi Formation Goodland Limestone Antlers Formation
Permian		Stratford Formation
Pennsylvanian	Post-Simpson or Geologic Units, Undifferentiated	Vanoss Group Ada Formation (Collings Ranch Conglomerate) Deese Group (Desmoinesian Series) Atoka Formation Wapanucka Limestone Springer Formation
Mississippian		Caney Shale Sycamore Limestone
Devonian		Woodford Shale Hunton Group
Silurian		
Late Ordovician		Sylvan Shale Viola Group
Middle Ordovician	Simpson Group	Bromide Formation Tulip Creek Formation McLish Formation Oil Creek Formation Joins Formation
Early Ordovician	Arbuckle Group	West Spring Creek Formation Kindblade Formation Cool Creek Formation McKenzie Hill Formation Butterly Dolomite Signal Mountain Formation Royer Dolomite Fort Sill Limestone
Late Cambrian		
	Timbered Hills Group	Honey Creek Limestone Reagan Sandstone
Middle Cambrian	Colbert Rhyolite	
Mesoprotenozoic	Tishomingo Granite, Trop Granite, granodiorite, and granitic gneiss	

Table 1: Chronostratigraphic and lithostratigraphic chart of the basement rock, Arbuckle Group, and Simpson Group of Oklahoma (modified from Christenson et al., 2011).

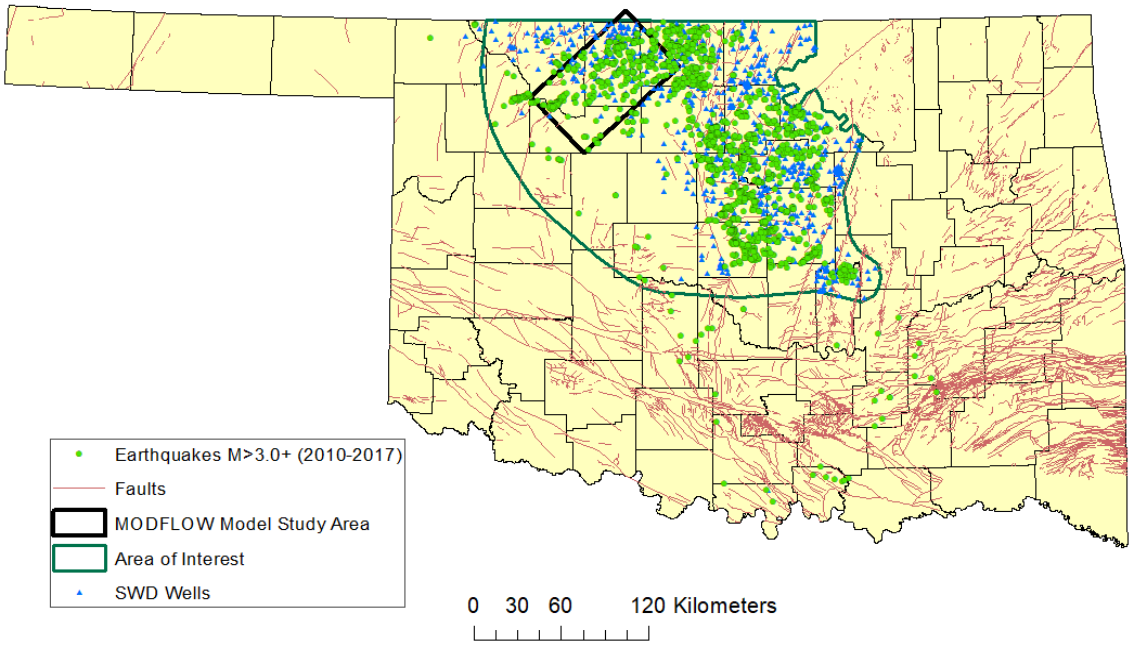


Figure 1: Study area in north-central Oklahoma. Cataloged faults from Oklahoma Geological Survey fault database (Marsh and Holland, 2016).

Chapter 4: Current Study

4.1 Study Area

North-central Oklahoma has a high rate of seismicity and concurrent high rates of SWD. Because of the correlation between Class II UIC Arbuckle SWD rates and seismicity in north-central Oklahoma, the Oklahoma Corporation Commission (OCC) issued directives for Arbuckle SWD in the Area of Interest (AOI) (Figure 1). The study area for this research is within the AOI, namely Alfalfa and Grant Counties and part of the Anadarko Shelf geologic province, which is a structurally distinct area (Northcutt and Campbell, 1995). Faults in the study area were designated as barriers or conduits to flow during numerical simulations to understand the dynamic pressure of the subsurface. The Fairview earthquake sequence, in the southwestern part

of the study area began in January 2016 and included five earthquakes before the M 5.1 mainshock 78 km (48 mi) outside of Fairview, OK (Yeck et al., 2017). The main earthquake and foreshocks occurred along a fault striking 40° east of north which aligns with the stress-field of the region (Holland, 2013; and Yeck et al., 2017). Most aftershocks for the earthquake occurred southwest of the M 5.1 epicenter, on a 6 km (3.7 mi) fault segment in the basement (Yeck et al., 2017). The epicenter and corresponding hypocenters of the earthquakes within this swarm were gathered from the USGS Earthquake Catalog and analyzed with pressure modeling results (http://www.ou.edu/ogs/research/earthquakes/catalogs).

4.2 Injection History

A state-scale compilation showed that the Arbuckle Group accepted less than 500 million barrels (79 million m^3) of wastewater in 2009 and over one billion barrels (158 million m^3) in 2014 (Murray, 2015). Because seismic activity was spatially and temporally correlated with the increase in SWD into the Arbuckle, regulatory actions were implemented to reduce Arbuckle SWD rates. In 2015, the OCC required operators to plug wells back from basement and for those operating Arbuckle SWD wells near earthquake epicenters to reduce disposal volumes or shut-in. After the Fairview earthquake sequence, the OCC reduced disposal volumes an average of 18% for 27 SWD wells in the Fairview region (Yeck et al., 2018).

This study area and model domain include 113 SWD wells and six monitoring wells that are completed within the Arbuckle. Injection histories (volume per month) for the Class II UIC SWD wells were collected from the online OCC Oil and Gas data files (http://www.occeweb.com/og/ogdatafiles2.htm). An SWD well is located 7 km (4 mi) away from the location of the Fairview earthquake sequence, but the majority of active Arbuckle SWD

wells are tens of kilometers from the Fairview sequence. Four SWD wells near the Kansas-Oklahoma border are also included in this study. The monthly/annual injection volumes for these wells were collected from the Kansas Geological Survey Fluid Injection Database (http://www.kgs.ku.edu/Magellan/Qualified/fluid.html).

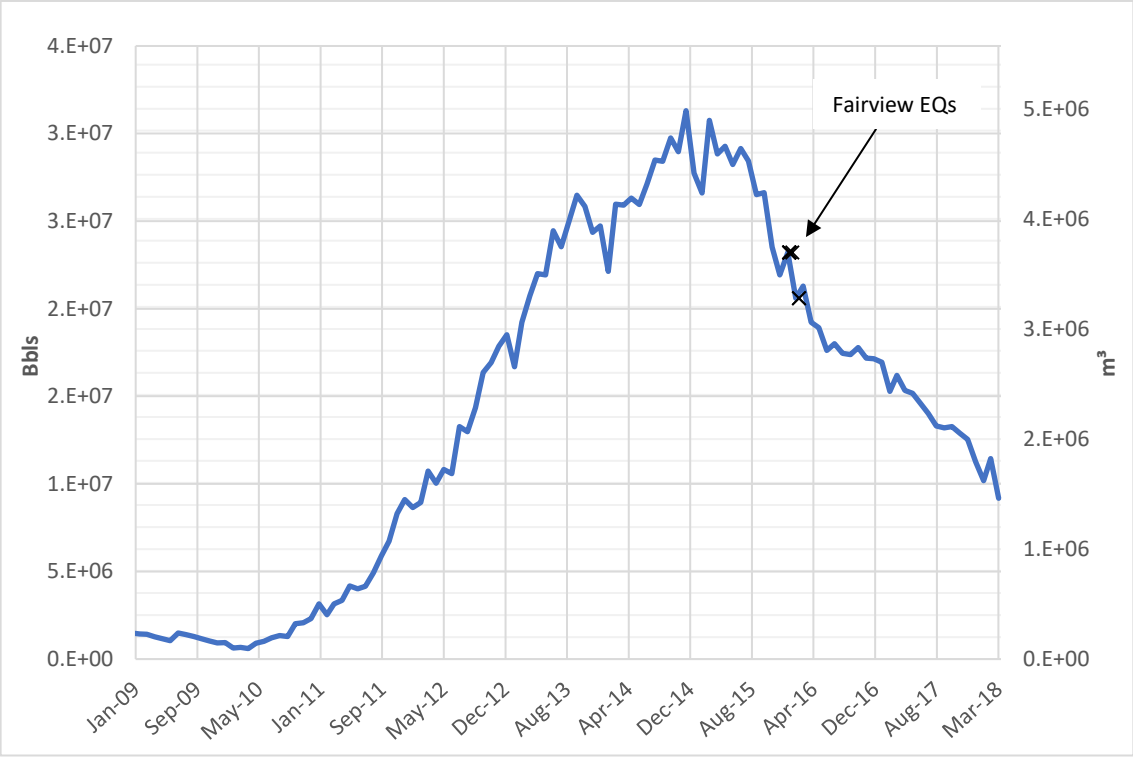


Figure 2: Cumulative injection volumes for saltwater disposal wells in model domain (Fairview region).

4.3 Downhole Pressure Monitoring

Although there has been a decrease in seismicity since the OCC implemented reductions, management strategies must be post-audited for their effectiveness. In August 2016, the Oklahoma Geological Survey began the Monitoring and Analysis of Arbuckle Group Pressures project. Fifteen inactive Arbuckle SWD wells were instrumented with Solinst Model 3001 LT Levelogger Edge M100:F300 pressure transducers roughly 25 m below the fluid level in the

well. After recording baseline fluid levels, downhole pressure and temperature readings were collected every 30 seconds since deployment of the transducers. The data are retrieved from the pressure transducers every month, post-processed, and normalized to elevation above sea level. The model output data (i.e., simulated head in the Arbuckle) is compared to observed pressure/head and used in the calibration process.

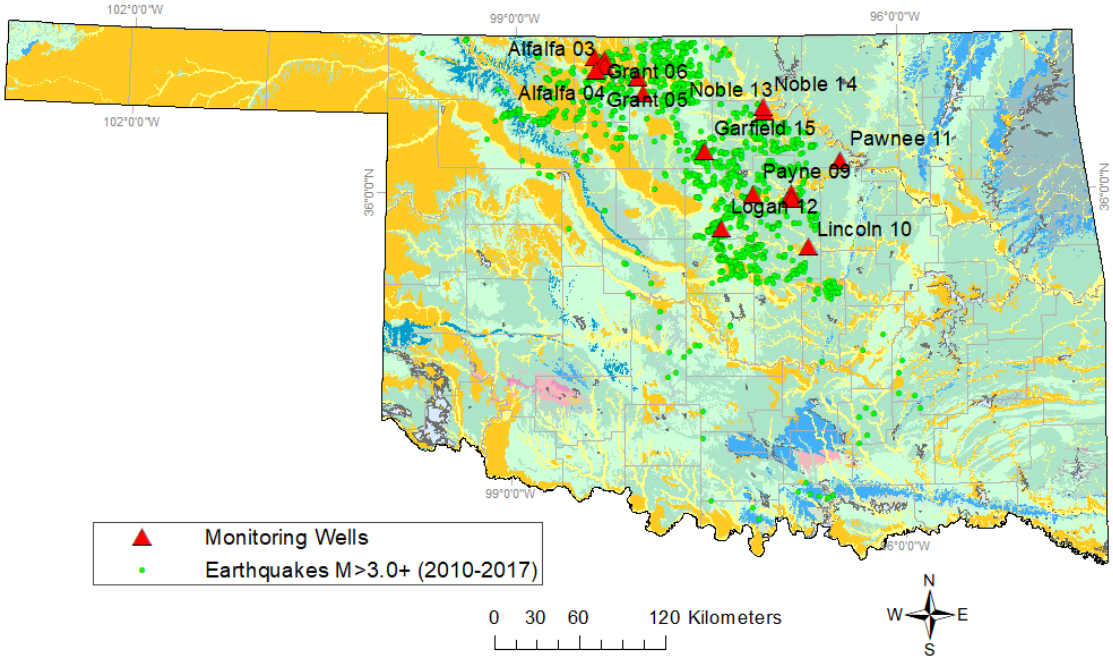


Figure 3: Pressure monitoring wells instrumented by the OGS in the Monitoring and Analysis of Arbuckle Group Pressures project. Fifteen wells are instrumented and continuously measuring pressure and temperature every 30 seconds.

Well	API	County	Lat	Long
Alfalfa 01	3500323106	Alfalfa	36.871139	-98.371500
Alfalfa 02	3500322737	Alfalfa	36.853908	-98.289931
Alfalfa 03	3500323033	Alfalfa	36.812417	-98.295472
Alfalfa 04	3500322247	Alfalfa	36.783944	-98.367306

Grant 05	3505322987	Grant	36.739417	-98.036444
Grant 06	3505322487	Grant	36.637667	-97.991750

Table 2: Geographic locations and API numbers of the six pressure-monitoring wells located within the study area/model domain.

4.6 Research Objectives

The general objective of this research is to adequately represent the hydrogeology and hydraulic properties of the Arbuckle Group and the overlying and underlying units so that recent pressure observations can be accurately matched when simulating reported monthly injection rates. The model can be used to understand how changes in injection rates have influenced pressure propagation through space and time (4D) in a region where earthquakes hypocentrally located in the basement are potentially induced by fluid-injection. This project will be instrumental in further understanding the heterogeneity and anisotropy of the reservoir because geologic conditions and constraints affect fluid pressure propagation within the Arbuckle and into basement zones. Additionally, the stratigraphic and hydrogeologic controls that influence the time delay between injection and pressure propagation will be explored alongside the Fairview earthquake sequence. This study is expected to test the role of fault zones in pressure propagation within the Arbuckle Group and Timbered Hills-Basement system along with confirming the hydraulic connection between the disposal and seismogenic zones.

Chapter 5: Methodology

5.1 Build Conceptual Model

A 3D geologic framework was developed to conceptualize stratigraphic layers and fault geometry of the model area. Subsurface geologic reports and maps, geophysical logs, and drill-

hole reports were used to construct the geologic framework (Crain and Chang, 2018). The geologic framework is represented with four hydrostratigraphic layers of similar hydraulic properties from top to bottom: Post Silurian, Silurian to Middle Ordovician, Arbuckle Group, and Timbered Hills-Basement rock. The layers are continuous and isotropic throughout the model domain.

5.1.1 Define Model Layers

Formations tops were estimated from well completion reports for the monitoring wells. The top elevation of the Arbuckle Group ranges from -1249 m (-4100 ft) to -2347 m (-7700 ft) and the elevation of the basement rock ranges from -1585 m (-5,200 ft) to 2743 m (-9,000 ft) within the study area. The total thickness of the four-layer model will be about 9400 km.

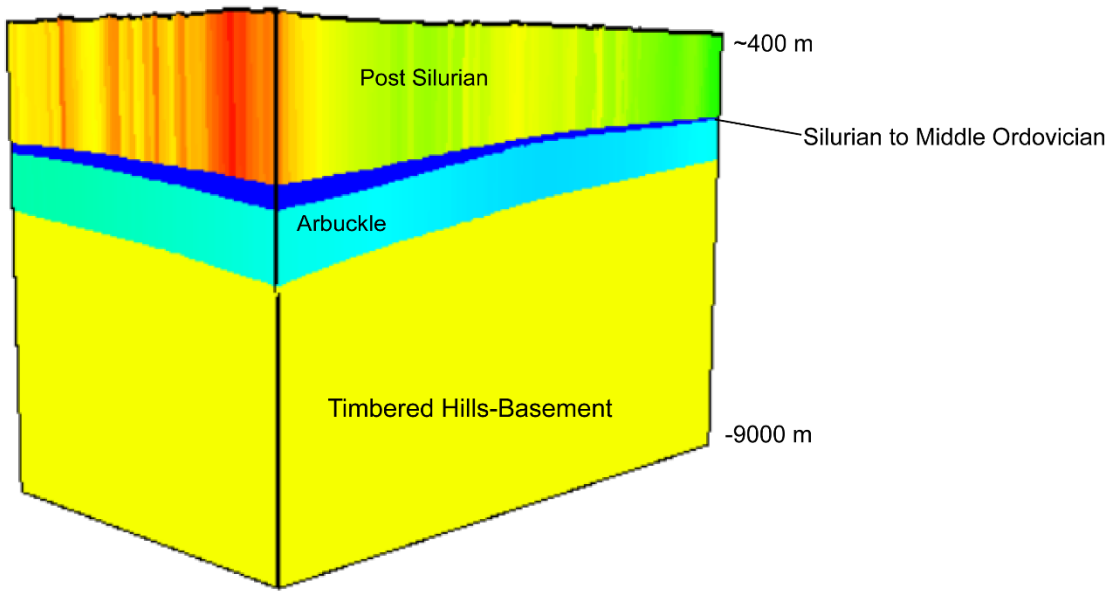


Figure 4: Model layers defined in ModelMuse with elevation of the model about 400 m and bottom depth of the four-layer model at -9000 m.

5.1.2 Define Layer Properties

Hydraulic conductivity is a function of both the fluid and the porous medium through which the fluid flows.

$$K = k\frac{pg}{\mu}$$

Where:

K=hydraulic conductivity (cm/s)

k=intrinsic permeability (cm^2)

p= density of the fluid (g/cm^3)

g=acceleration of gravity (cm/s^2)

v= viscosity of fluid (g/s*cm)

Hydraulic conductivity and other reservoir properties are dependent on the properties of the formation water. Studies on formation waters in Oklahoma show that total dissolved solids (TDS) concentration increase with depth. TDS of produced water from Oklahoma reservoirs has a median concentration of about 180,000 ppm in the USGS National Produced Waters Database (Blondes at al., 2017). The compressibility of brine is the inverse of bulk modulus, which is a function of pressure, temperature, and salinity (Batzle and Wang, 1992). The formation water and the rock matrix will contract and expand with changes in hydraulic head within a confined reservoir.

Disposal water properties	180000 ppm
Density (kg/m³)	1136
Gravity (m/s²)	9.8
Viscosity (kg/m*s)	6.71E-04
Specific weight (kN/m³)	111143
Avg. temp (°C)	65
N=kg*m/s²	

Table 3: Disposal water properties from the U.S. Geological Survey National Produced Waters Geochemical Database (Blondes et al., 2017; and Dessouky and Ettouney, 2002).

Previous hydrogeological modeling studies of the Arbuckle in Oklahoma used a similar hydrostratigraphic conceptual framework, with the top layer representing post-Simpson strata (Carrell, 2014; and Christenson et al., 2011). For this study, the layer is better represented as the time-stratigraphic unit “Post Silurian” (PS).

Directly under the Post Silurian layer is the Silurian to Middle Ordovician (S to MO) model layer that includes the Simpson Group and some additional units above the Simpson Group including the Viola Group, Sylvan Shale, and Hunton Group. The Hunton Group lies directly under the Woodford Shale, which is laterally continuous and of low permeability. The Hunton Group is described as having extensive fractures and karsting in the upper 15 ft (4.5 m) of the group (Milad and Slatt, 2017). The Silurian to Middle Ordovician model layer is highly heterogenous with interbedded layers of shale between carbonate and sandstone formations. The model layer is assigned a low vertical hydraulic conductivity value (3.048E-13 m/d), but a relatively high horizontal conductivity value (3.2E-02 m/d).

Carrell (2014) obtained hydraulic conductivity values for Oklahoma basement rock in the Cherokee Platform from drill-stem tests on SWD wells injecting at deep depths. Although the matrix of crystalline rock has very low permeability, fractures and faults can increase the hydraulic conductivity of the rock. Literature values for fractured igneous rock are around 6.91E-04 m/d while unfractured igneous rock hydraulic conductivity can be as large as 2.59E-09 m/d (Domenico and Schwartz, 1990). Initial properties of the Timbered Hills-Basement layer are based on pervious studies in north-central Oklahoma that use 9.144E-04 m/d and 4.57E-04 m/d values for the Basement horizontal and vertical hydraulic conductivity, respectively.

5.1.3 Compile Arbuckle Group Data

Previous investigations provide properties of the Arbuckle Group at various spatial scales; therefore, more data exists to establish an appropriate range of properties for the Arbuckle model layer. In addition to large-scale permeability studies from pressure data, small-scale permeability and porosity values have been collected from core studies and laboratory analyses of core plugs from wells near the study area. Williams (2017) studied cores/core plugs and logs from wells in the Cherokee Platform. The core plugs were sent to the Integrated Core Characterization Center (IC3) and Integrated Poromechanics Institute (iPMI) for analysis of permeability, static and dynamic compressibility, and porosity.

Using a hand-held permeameter, TinyPerm II, small-scale permeability measurements were also collected from the Union Texas Idema core extracted from Cleveland County, Oklahoma. Previous numerical models of the Arbuckle Group established sub-layers within the group to represent hydrostratigraphy of the zone.

A solid earth-tide study was conducted to evaluate pressure fluctuations in the Arbuckle resulting from tidal strain. Using a Fourier transforms technique, the permeability, matrix compressibility, porosity, transmissivity, storage coefficient, and specific storage were estimated for the Arbuckle Group rock.

Tidal strain analyses can be used to estimate properties of confined and unconfined aquifers (Perilla, 2017). The mean specific storage value (1.39E-06 m^{-1}) and the mean storativity value (3.69E-04) calculated by Perilla (2017) are one to two orders of magnitude lower than previous Arbuckle-Simpson aquifer studies (Christenson et al., 2011).

Well	Tidal Component	Specific Storage (m-1)	Storage coefficient (dimensionless)	Transmissivity (m2/d)	Barometric Efficiency (dimensionless)	Porosity (percentage)	Matrix Compressibility (psi-1)	Hydraulic Conductivity (m/s)	Intrinsic Permeability (mD)	Hydraulic Diffusivity (m2/s)
Alfalfa 03	O1	1.50E-06	1.13E-03	12.07	0.42	16%	6.18E-07	1.87E-07	29.03	3.87
	M2	6.11E-07	4.60E-04	6.72		7%	2.52E-07	1.04E-07	16.16	4.91
Alfalfa 04	O1	2.66E-06	8.18E-04	3.75	0.74	52%	4.94E-07	1.42E-07	22.08	0.05
	M2	2.00E-06	6.14E-04	2.09		39%	3.71E-07	7.90E-08	12.29	0.04
Grant 06	O1	2.34E-06	1.05E-03	375.48	0.87	54%	2.21E-07	9.78E-06	1520.89	4.17
	M2	1.28E-06	5.71E-04	194.11		29%	1.20E-07	5.05E-06	786.23	3.95
Lincoln 10	O1	2.20E-06	2.57E-03	18.77	0.68	39%	5.03E-07	1.87E-07	29.06	0.08
	M2	8.93E-07	1.04E-03	13.44		16%	2.04E-07	1.34E-07	20.8	0.15
Pawnee 11	O1	1.28E-06	2.14E-04	14.44	0.61	21%	3.51E-07	1.00E-06	155.84	0.78
	M2	3.38E-07	5.67E-05	8.20		5%	9.26E-08	5.69E-07	88.43	1.68
Logan 12	O1	1.80E-06	6.74E-04	14.72	0.54	26%	5.83E-07	4.58E-07	71.26	0.25
	M2	4.30E-07	1.61E-04	8.20		7%	1.39E-07	2.55E-07	39.67	0.59
Median		1.39E-06	6.44E-04	12.76	0.65	24%	3.02E-07	2.21E-07	34.37	0.69

Table 4: Arbuckle properties derived from earth tide analysis of pressure monitoring data (Perilla, 2017).

Additionally, injection rates were provided by well operators for active SWD wells near multiple pressure-monitoring wells and used to calculate Arbuckle hydraulic properties. A modified Theis equation was used to derive properties of the Arbuckle Group, using hourly injection data for a well near Alfalfa_02, by adjusting unknown parameters (e.g., specific storage, transmissivity, thickness, radial distance) to match the Theis solution to the observations in Alfalfa_02. The best-fitting values for hydraulic conductivity and specific storage were 2.1 m/d and 4.58E-07 m^{-1}, respectively.

5.1.4 Identify Arbuckle Facies

Extensive studies in Kansas conducted to improve enhanced oil recovery (EOR) methods also explore the Arbuckle as a potential CO_2 reservoir. The intertidal and subtidal strata of the Arbuckle Group are highly dolomitized and heterogenous with smaller zones with high permeability imbedded in lower permeability sections (Franseen, et al., 2012; Carr et al., 1986; and Puckette, 2009). Although karsting and fracturing are important factors affecting production potential of the Arbuckle Group, distribution of lithofacies and packaging of laterally-extensive strata is also important, because matrix porosity and permeability can highly influence hydraulic properties. Three identified reservoir architectures within the Arbuckle Group a) permeability of group of strata is controlled by fractures b) both lithofacies and fractures result in complex porosity and permeability and c) lithofacies control hydraulic properties of the rock because fracturing and karstification are limited (Franseen et al., 2012). Non-reservoir facies are prominent in the lower section of the Arbuckle (Franseen et al., 2004).

5.1.5 Define Layer Pressure/Hydraulic Head

Initial pressure head measurements for the Arbuckle needed to be established as a baseline condition to anticipate increase in pressure related to high disposal rates. Through drill stem test analysis of wells across the state, Puckette (1996) calculated bottom-hole pressures from oil and gas wells and made a potentiometric surface map of the Arbuckle Group. Using Dahlberg's formula, the bottom-hole pressure from well logs was used to calculate potentiometric head values, all normalized to sea level (Dahlberg, 2005). Potentiometric head values illustrate the driving force or hydraulic gradient, which is important for wastewater disposal because it dictates the direction that wastewater would flow, or pressure would propagate from high potential energy to low potential energy. This potential energy gradient will dictate how fluids may flow from the disposal zones into surrounding reservoirs, that are in hydraulic communication (Puckette, 1996).

The equation for potentiometric/hydraulic head (Fetter, 2001):

$$h = z + \frac{P}{pg}$$

h= hydraulic head (m)

z= elevation (m)

P= pressure elevation (N/m^2)

p= density of water (g/m^3)

g= gravity (m/s^2)

The potentiometric surface map from Puckette (1996) was digitized using ArcGIS, and values were interpolated across the model domain to obtain pre-development hydraulic head values for the Arbuckle. These values acted as initial conditions for the steady-state model. Post

Silurian and Silurian to Middle Ordovician layers will be considered hydrostatic like other modeling studies. Carrell (2014) analyzed drill stem tests to calculate hydraulic head values of the Simpson Group prior to saltwater disposal and found the group to be underpressured, most likely from oil and gas production (Al-Shaieb and Puckett, 2003). The difference in pressure between the Simpson Group and surrounding layers confirms a low vertical hydraulic conductivity. The Post Silurian and Timbered Hills-Basement layers are both considered hydrostatic, meaning the hydraulic head of the layer is nearly coupled with the land surface (Bredehoeft et al., 1992).

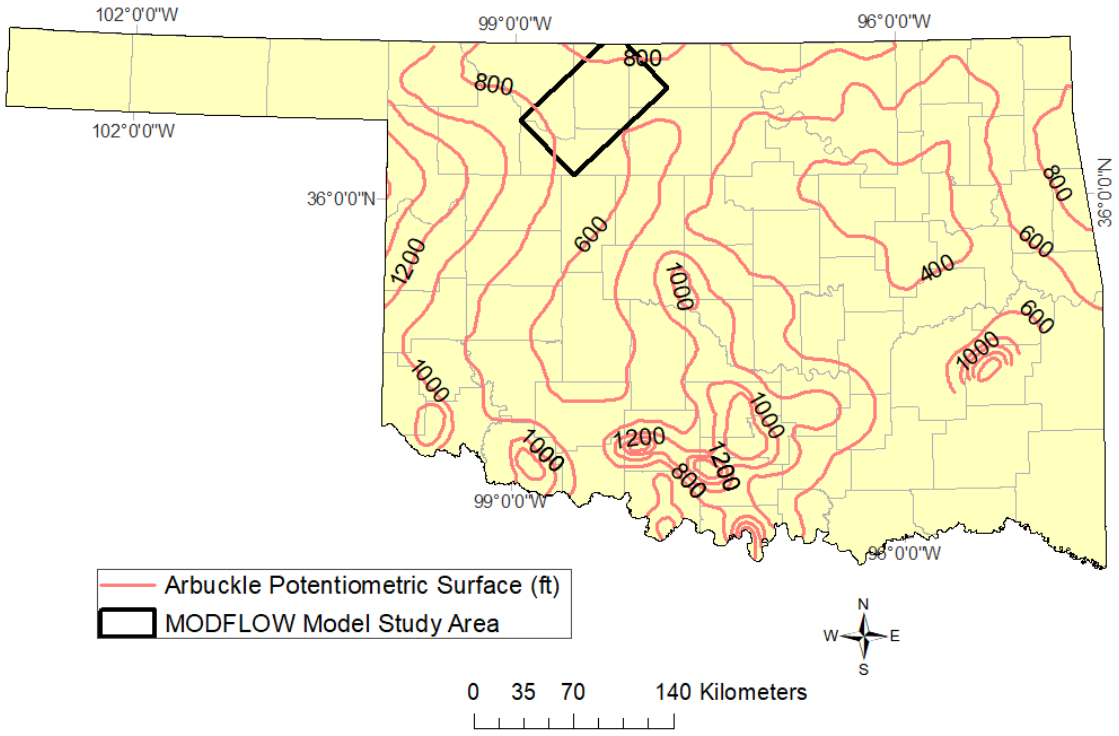


Figure 5: Potentiometric surface map of Oklahoma compiled by Puckette (1996). The hydraulic head values are used as the initial conditions for steady-state modeling.

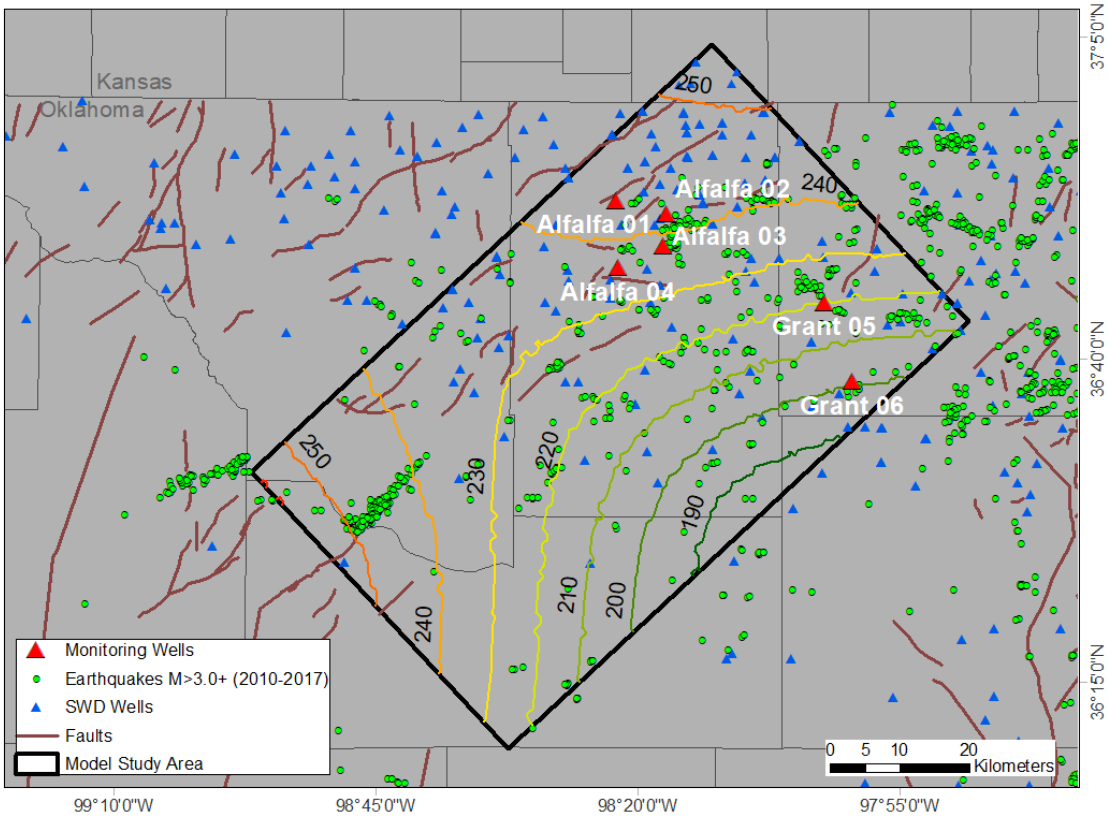


Figure 6: Model domain for the numerical simulations using MODFLOW (Harbaugh, 2005). Model area dimensions include 54 km x 90 km area (4860 km²) including 113 SWD wells, six monitoring wells, and faults from Oklahoma Geological Survey Fault database (Marsh and Holland, 2016). Initial head contours (m) from Puckette (1996).

5.1.6 Identify Geologic Structures

One of the objectives of this study is to understand how fracture/fault patterns in the strata promote or impede pore pressure propagation from SWD wells. Faults were mapped in the model domain to investigate the impacts of these structures acting as conduits or barriers to flow. Current mapped faults are cataloged in the Oklahoma Geological Survey Fault Map Database, but many recent earthquakes in Oklahoma have occurred on unmapped faults (Marsh and Holland, 2016; and Zoback and Alt, 2017). The Fairview earthquake sequence occurred on a 14 km (8 mi) long fault that is partially unmapped (McGarr and Barbour, 2017; and Yeck et al.,

2016). A better assessment of the faults and geologic structures in the seismically active areas (i.e. north-central Oklahoma) is necessary to understand injection-induced seismicity (Zoback and Alt, 2017).

5.2 Numerical Model

Model simulations are performed using the USGS groundwater modeling code, MODFLOW 2005 and the graphical user interface, ModelMuse (Harbaugh, 2005). Graphical user interfaces (e.g., ModelMuse) are program packages that simplify the creation of the input files for the model and reading the output files. A finite-difference method is used to solve the partial differential equation governing groundwater flow across a discretized model domain for approximated head values.

$$\frac{\partial}{\partial x}\left(K_{xx}\frac{\partial h}{\partial x}\right)+\frac{\partial}{\partial y}\left(K_{yy}\frac{\partial h}{\partial y}\right)+\frac{\partial}{\partial z}\left(K_{zz}\frac{\partial h}{\partial z}\right)+W=S_s\frac{\partial h}{\partial t}$$

with K_{xx}, K_{yy}, and K_{zz} are hydraulic conductivity along x, y, and z coordinate axes; h is hydraulic head; W is volumetric flux per unit volume, S_s is specific storage, and t is time.

This equation combines Darcy's law in 3-dimensions and the continuity equation. The volume outflow rate equals the volume inflow rate and the release of water from storage for transient flow (Wang and Anderson, 1982). A few model assumptions and limitations for MODFLOW numerical modeling includes that water has a constant density, dynamic viscosity, and temperature and the principal components of anisotropy of the hydraulic conductivity tensor do not include non-orthogonal anisotropies that may result from, for example, highly fractured rocks.

$$K = \begin{matrix} Kzz & 0 & 0 \\ 0 & Kyy & 0 \\ 0 & 0 & Kzz \end{matrix}$$

Geologic units at the scale of a regional model are heterogeneous and anisotropic; therefore, hydraulic conductivity could vary in different directions of the model. Data for the three-principal component of the hydraulic conductivity tensor are needed to accurately quantify the anisotropy of a reservoir (Anderson and Woessner, 1992). Vertical anisotropy results from laminae and bedding planes and usually limits the flow of water perpendicular to the hydrostratigraphic layers in the model (Anderson and Woessner, 1992), so Kx/Kz ratio generally ranges from 1-1000. Horizontal anisotropy (Kx/Ky) can be caused by fractures sets and sedimentary structures and is typically much lower than vertical anisotropy (Anderson and Woessner, 1992).

5.3 Setup Steady-State Model

5.3.1 Model Domain

The study area/conceptual model will be transformed into a spatially discretized model domain for numerical modeling. Establishing the cell size for a groundwater model domain allows for defining important geologic features in the model framework and appropriately representing features to avoid errors and biases in modeling results (Reilly and Harbaugh, 2004). The total area of the model domain is 4680 km²; each cell of the model is 1 km² forming a 54 km x 90 km rectangular grid (Figure 4). A coarse grid is not appropriate to collect accurate head values from monitoring wells located near injection wells. Model cells containing both a monitoring well and injection well(s) (ex. Alfalfa 1) were subdivided until wells were in different cells. Layer elevations

were based on elevations published as open-file reports by the Oklahoma Geological Survey (Crain and Chang, 2018). Using ArcGIS, the contours for the top of the Basement rock/ bottom of the Arbuckle and the top of the Hunton Group were converted into raster files and imported into ModelMuse as elevations for each model layer. There are four layers within the model including the Timbered Hills-Basement, Arbuckle, Silurian to Middle Ordovician, and Post Silurian. The Timbered Hills-Basement layer is vertically discretized from the base hydrogeological model, but still considered one hydrostratigraphic unit.

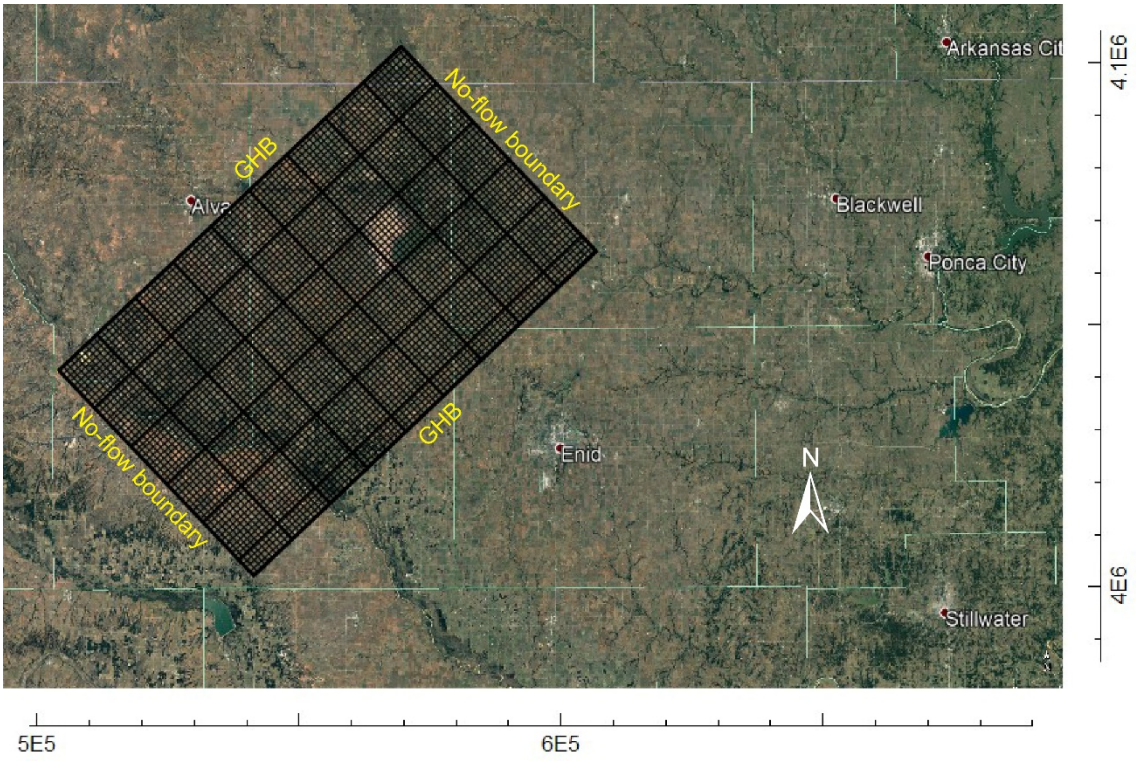


Figure 7: Model domain discretized for the numerical simulations using MODFLOW (Harbaugh, 2005). Model area dimensions include 54 km x 90 km (4860 km^2) and each cell is 1 km^2.

5.3.2 Boundary Conditions

A numerical model simulates groundwater flow using governing equations, boundary conditions, and starting heads/initial conditions (Anderson and Woessner, 1992). Boundary

conditions mathematically determine the head/flux at the bounds of the model. Ideally, model boundaries will represent physical or hydraulic features that affect the flow system, but this option is not always feasible. This model is considered a mixed problem with both head-dependent flux boundaries and no-flow or streamline boundaries laterally bounding the model domain. Vertically, the model will be bounded by sealing stratigraphic units found in the overlying Simpson Group and underlying basement rock. Natural hydraulic barriers (no-flow boundaries) are present on the northeast and southwest sides of the model domain, representing a natural "high" in the Arbuckle regional hydraulic head. The northwest and southeast sides of the domain are general-head boundaries (GHB) that calculate the flow across the boundary given the head value of the boundary (Anderson and Woessner, 1992).

5.3.3 Input Parameters

Representative reservoir characteristics of the Arbuckle Group and the surrounding zones are essential for proper modeling and evaluation. The Arbuckle layer is considered fully saturated with nonturbulent flow. All layers within the model domain are represented as a confined aquifer/reservoir. Starting hydraulic properties (i.e., prior to model calibration) are based on previous studies of the Arbuckle Group in northern Oklahoma (Carrell, 2014; and Perilla, 2017). Hydraulic properties used in the model include horizontal/ vertical hydraulic conductivity, vertical anisotropy, and specific storage. Numerous studies and literature sources provide petrophysical and hydraulic properties of the Arbuckle Group (Christenson et al., 2011; Kroll et al., 2017; Perilla, 2017; and Williams, 2017). Hydraulic properties within a geologic unit can differ by orders of magnitude; therefore, values of hydraulic conductivity are usually stated as ranges (Christenson et al., 2011).

Model Layer	Post Silurian	Silurian to Middle Ordovician	Arbuckle	Basement
Initial Kh (m/d)	3.05E-05	0.032	0.019	9.14E-04
Initial Kv (m/d)	3.05E-13	3.05E-13	2.77E-01	4.75E-04
Avg. layer top (m)	417	-1638	-1808	-2334
Thickness (m)	2056	169	526	6666
Initial Head Values (m)	417	100	Puckette, 1996	417

Table 5: Summary of model inputs and initial parameters for the model based on previous studies (Puckette, 1996; Carrell, 2014; and Perilla, 2017).

For the steady-state model, the amount of water flowing into the representative model domain or an individual cell equals the amount of water flowing out (Wang and Anderson, 1982). Running a steady-state model includes head being independent of time and lacks a storage component.

Initial scenarios run for the model were under steady-state conditions to evaluate the construction of the model. It is assumed that predevelopment water levels do not vary from pressure measurements interpreted by Puckette (1996). The stress period will be one single time step with the storage term equal to zero, representing the system prior to wastewater disposal. Steady-state simulations allow for a range of hydraulic conductivities to be established for each layer of the model. The steady state model does not include the faults and fracture zones in the model domain because faults were not accounted for in the Puckette (1996) representation of the Arbuckle's "virgin" pressure. However, the fracture zones and faults are added to the transient model so that the model can be calibrated to match simulated and observed heads. Steady-state model calibration is performed to convergence, and a steady-state water budget that simulates starting head values of the conceptual model. The calibration process includes a sensitivity

analysis where hydraulic conductivity values are altered to test the sensitivity of the model (how much the parameters affect the simulation results). The simulated steady-state model hydraulic head values become the initial conditions for the transient model.

5.4 Setup Transient Model

The initial conditions for the transient model are the resulting model parameters from the steady-state calibration process. The transient model includes 113 SWD wells that inject into the Arbuckle from January 2009–April 2018 and mapped faults from the Oklahoma Geological Survey (OGS) fault database (Marsh and Holland, 2016). The z-coordinates for SWD wells in the model domain are located at the bottom of the injection interval. For SWD wells in Oklahoma, the injection depths were recorded on well logs to be below the "top of the basement" that was estimated by Change and Crain (2018). Because the injection depth at a specific well is likely more accurate than the regional-scale estimate of top of basement, the “conceptual model” was adjusted and the geologic framework modified by extending the Arbuckle layer in the model 500 m into the basement. Operational inputs include 113 SWD wells and six monitoring wells all completed within the Arbuckle Group. All faults are represented as head- dependent internal boundary conditions within the model domain and have a width of one cell (1 km).

During the model time frame, eight SWD wells are plugged-back to inject in shallower formations and essentially no longer active in the model after being recompleted. Initial transient model simulations do not include faults and fracture zones. Hydraulic parameters and input data unique for transient simulations include specific storage, initial conditions, hydrologic stresses acting as sources and sinks (e.g., disposal wells and faults), and time (Anderson and Woessner, 1992).

5.4.1 Specific Storage

During wastewater injection in the modeling scenarios, there will be a change in head values within the confined reservoir unit, water will either be expelled or stored (Fetter, 2001). When the hydraulic head in a confining layer declines, the matrix compresses. The specific storage (Ss) (the elastic storage coefficient) is the amount of pore water expelled or taken into storage in response compression of the rock matrix or water per unit change in head (Fetter, 2001). This applies to both saturated and unsaturated beds.

$$S_S = \rho_w g(\alpha + n\beta)$$

ρ_w= density of the water (g/m³)

g= acceleration of gravity (m/s²)

a= compressibility of the rock matrix (N/m^2)

n= porosity

β= compressibility of the fluid (N/m^2)

Geomechanical and seismological studies of the Arbuckle Group have produced values for the porosity and rock compressibility used for calculating specific storage (Barbour et al., 2017; and Kroll et al., 2017). Classic literature values of S_s range from 9.18E-04 m^{-1} for hard clay to greater than 3.28E-06 m^{-1} for unfissured rock (Domenico and Mifflin, 1965). From injection tests (i.e., observed pressure change in monitoring well resulting from nearby active injection well) on Alfalfa_01 and Alfalfa_02, S_s value for the Arbuckle was 4.53E-07 m^{-1} which is slightly lower than values previously derived for the Arbuckle in Oklahoma and Arkansas (Perilla, 2017; Ogwari and Horton, 2016; Christenson et al., 2011; and Carr et al., 1986).

Three transient model scenarios are used to simulate years 2009 – 2018 and pressure observed during 2016 and 2017. Scenarios include:

Scenario 1: Sub-divide Arbuckle into sub-layers;

Scenario 2: Change fault permeability and size; and

Scenario 3: Alter properties of individual and inferred faults

Simulations will run for transient conditions representing the years 2009 – 2018, producing a distribution of hydraulic head values for the model area during this time. Additionally, pressure changes will be recorded at the hypocenter of the Fairview earthquake mainshock and two other observation points placed within cells representing the Timbered Hills-Basement layer (Table 7) in the numerical model.

Obs. Points	Date	Latitude	Longitude	Depth	Magnitude	Detail
Fairview Main	2/13/2016	36.4898	-98.709	8.31 km	5.1	31km NW of Fairview, Oklahoma
Fairview 2	1/7/2016	36.4955	-98.7254	4.058 km	4.7	33km NW of Fairview, Oklahoma
Observation 1				4 km		~5km from both Alfalfa_04 & Alfalfa_05
Observation 2				3 km		Fairview region

Table 6: Observation points representing the locations of the Fairview mainshock, foreshocks, and additional locations/depths of interest. Simulated pressure at these locations will be evaluated and compared to seismic events in the Fairview sequence.

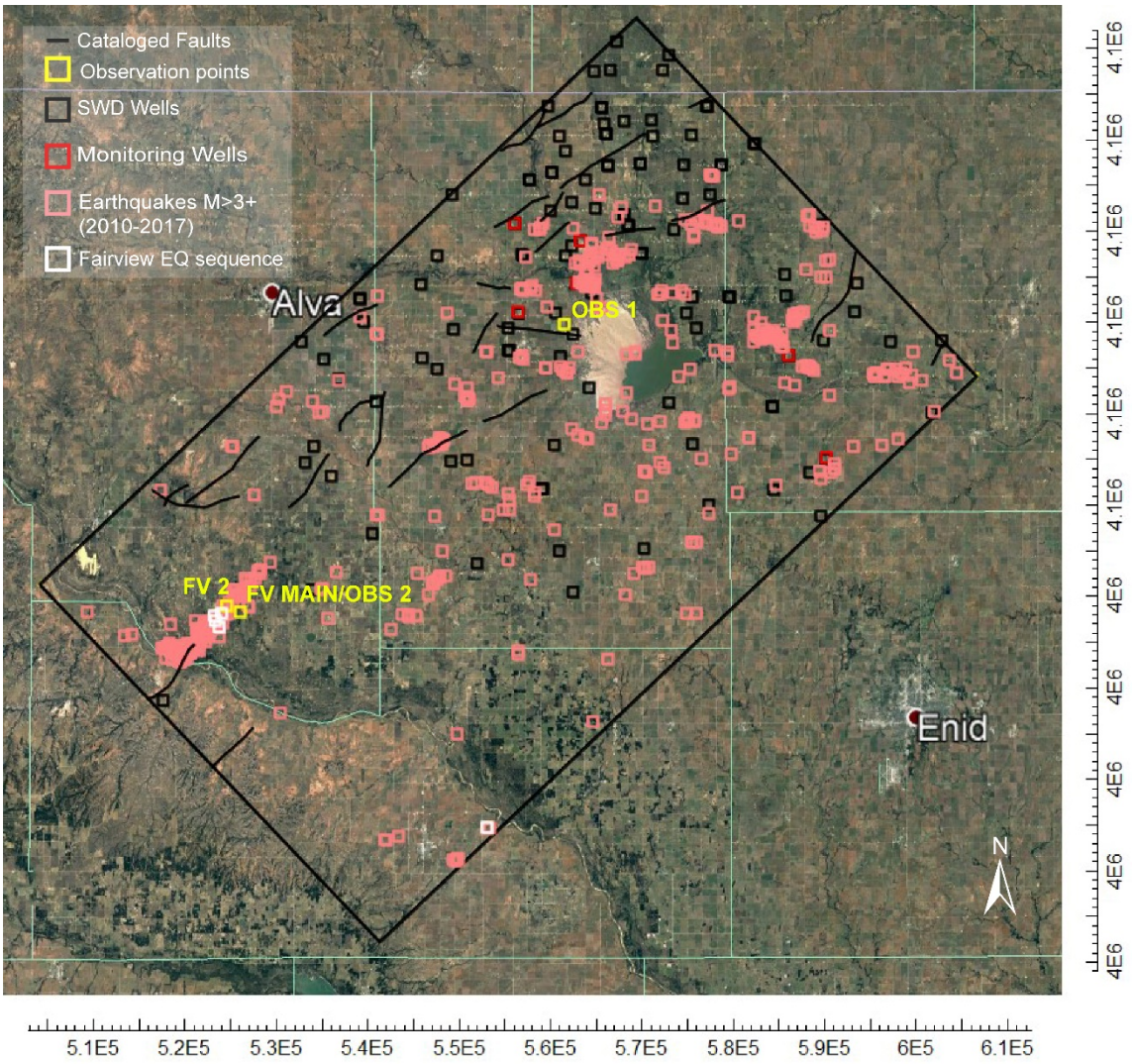


Figure 8: ModelMuse image of the model domain for transient model simulations. The observation points (Table 6) to compute pressure changes within the Arbuckle and Timbered Hills-Basement are highlighted in yellow.

5.4.2 Monitoring Well Data

Groundwater modeling is a method to represent a simplified system. This numerical modeling study strives to advance the current understanding regarding possible influence of fractures and fault zones on pore pressure diffusion from injection wells. The formal inverse modeling approach resolves hydraulic properties and relationships of the subsurface from measurements of hydraulic head (Anderson and Woessner, 1992). The model will be calibrated

against the six pressure monitoring wells within the model domain. The output file after running the model computes a residual which is the first estimate of change between the current solution and the last one.

Initial Head Values (m)	
A01	243.27
A02	241.93
A03	238.50
A04	235.62
G05	219.04
G06	200.17

Table 7: Initial head pressure values (m) at each monitoring well (Puckette, 1996).

5.4.3 Model Assumptions

Assumptions and simplifications were established during the development of the conceptual and numerical model. Limitations for properties of the groundwater (or disposal water) are intrinsic to the MODFLOW software. The water is held at a constant density and viscosity throughout the entire model domain. An additional assumption for the model, specific to this study, includes the Arbuckle as the sole SWD injection interval. Also, pressure from enhanced oil recovery (EOR) and SWD injection in shallower, overlying units does not interact with pressure regimes of the Arbuckle and Timbered Hills-Basement layer. The Post Silurian and Silurian to Middle Ordovician layers contain shale formations that act as hydraulic barriers to pressure migrating to lower model layers. This study also assumes the pressure data compiled by Puckette (1996) is an accurate representation of the hydraulic head values of the Arbuckle before SWD. The Arbuckle zone is assumed to be a laterally homogenous unit for this model. Proper data is not yet available for delineating aerially distributed (x,y) zones of the Arbuckle that have unique properties.

Chapter 6: Results

A groundwater flow model is calibrated by solving the groundwater flow equation with assumed model parameters to reproduce known conditions of the reservoir (Fetter, 2001). The calibration process requires modification of the model parameters until simulated head values closely match observed head values from the field (Reilly and Harbaugh, 2004). Measurements from the field or data used as initial values for model parameters can vary by orders of magnitude and need to be adjusted to represent the property at the scale of the model cells (Christenson, et al. 2011). Two techniques for calibrating a groundwater flow model include 1) manual trial-and-error and 2) automated parameter estimation using an external program to MODFLOW (Anderson and Woessner, 1992). This study uses a trial-and-error process for both steady-state and transient model calibration.

The sensitivity analyses adjusted parameters in sequential model runs to match simulated head to calibration targets including Puckette (1996) “virgin” heads for the steady-state model and 10 months of monitoring data (September 2016 – June 2017) for the transient model.

6.2 Steady-State Model Results

A sensitivity analysis is performed to determine how sensitive a model for simulating head is to changes in the model parameters including hydraulic properties and boundary conditions. From this, the uncertainty of the model can be understood, identifying which parameters affect the simulated head values (Fetter, 2001). The initial sensitivity analysis includes varying the hydraulic conductivity values of each model layer by two orders of magnitude while keeping the other parameters constant.

Initial Parameters	**Post Silurian**	**Silurian to Middle Ordovician**	**Arbuckle**	**Timbered Hills-Basement**	**R^2**
Kh (m/d)	3.05E-05	0.032	0.019	9.14E-04	0.9054
Kv (m/d)	3.05E-13	3.05E-13	0.00277	4.57E-04	
TH-B *vertical hydraulic conductivity decreased by three orders of magnitude (E-03)*					
Kh (m/d)	3.05E-05	0.032	0.019	9.14E-04	0.8927
Kv (m/d)	3.05E-13	3.05E-13	0.00277	4.57E-07	
A *hydraulic conductivity increased by two orders of magnitude (E02)*					
Kh (m/d)	3.05E-05	0.032	1.9	9.14E-04	0.8845
Kv (m/d)	3.05E-13	3.05E-13	0.277	4.57E-07	
A *hydraulic conductivity decreased by two orders of magnitude (E-02)*					
Kh (m/d)	3.05E-05	0.032	0.00019	9.14E-04	0.458
Kv (m/d)	3.05E-13	3.05E-13	0.0000277	4.57E-07	
B *horizontal hydraulic conductivity decreased by two orders of magnitude (E-02)*					
Kh (m/d)	3.05E-05	0.032	0.019	9.14E-06	0.8863
Kv (m/d)	3.05E-13	3.05E-13	0.00277	4.57E-07	
B *horizontal hydraulic conductivity increased by two orders of magnitude (E02)*					
Kh (m/d)	3.05E-05	0.032	0.00019	9.14E-02	0.893
Kv (m/d)	3.05E-13	3.05E-13	0.0000277	4.57E-07	
S to MO *horizontal hydraulic conductivity decreased by two orders of magnitude (E-02)*					
Kh (m/d)	3.05E-05	0.00032	0.019	9.14E-04	0.8927
Kv (m/d)	3.05E-13	3.05E-13	0.00277	4.57E-07	

Table 8: Resulting table of sensitivity analysis for steady-state model. Correlation coefficient is measured to compare simulated hydraulic head values for the Arbuckle Group to initial conditions from Puckette, 1996.

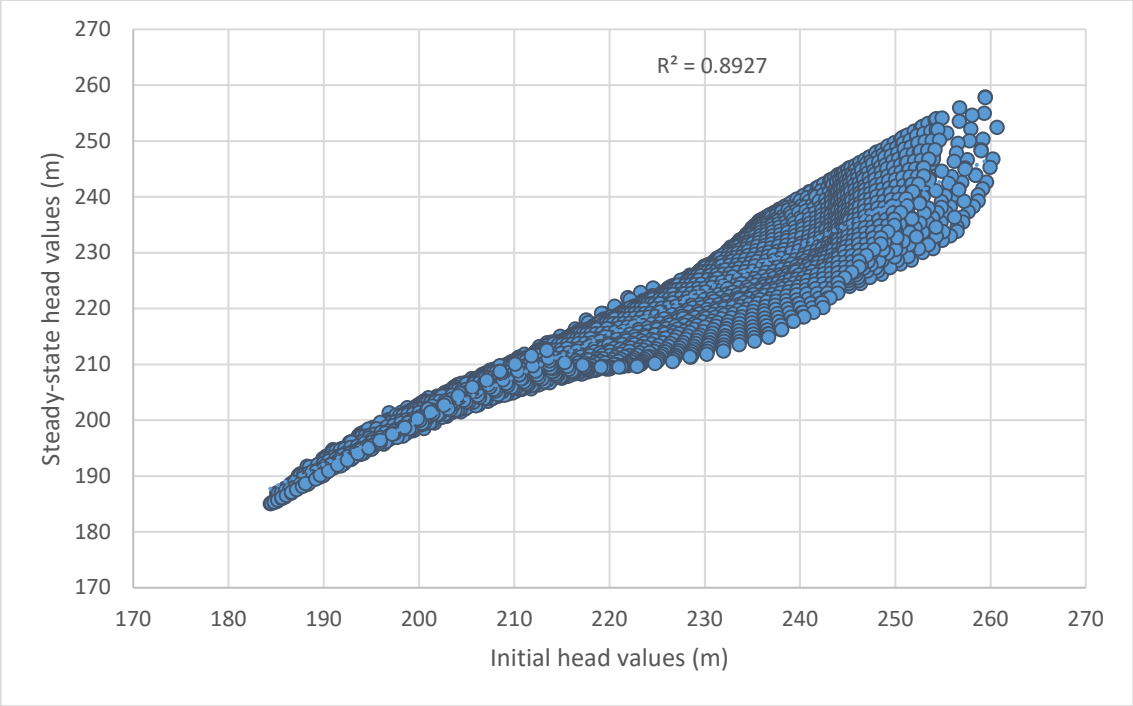


Figure 9: Assigned model parameters for initial steady state model against the initial hydraulic head values from Puckette, 1996

A larger vertical hydraulic conductivity value (4.57E-04 m/d) for the Timbered Hill-Basement layer, produces a large discrepancy between initial conditions and simulated head values during steady-state simulations for this model layer. The vertical hydraulic conductivity for the Timbered Hills-Basement fits initial conditions better at 4.57E-07 m/d instead of 4.57E-04 m/d. Although a larger vertical hydraulic conductivity value for this model layer aligns well with previous studies, a smaller Kv maintains Timbered Hills- Basement hydraulic head values within about 8 m of the initial conditions. There is little change in the correlation coefficient for the Arbuckle Group (initial conditions vs simulated values) when changing the horizontal hydraulic conductivity values of the Timbered Hills-Basement Layer and the Silurian to Middle Ordovician layer.

Initial Parameters	Post Silurian	Silurian to Middle Ordovician	Arbuckle	Timbered Hills-Basement
Kh (m/d)	3.05E-05	0.032	0.019	9.14E-04
Kv (m/d)	3.05E-13	3.05E-13	0.00277	4.57E-07
Ss (1/m)	8.00E-06	8.00E-06	4.53E-07	1.00E-07
Faults	None			

Table 9: Best fit hydraulic properties obtained from steady-state model calibration used for initial parameters of the transient model.

6.3 Transient Model Results

The sensitivity analysis for transient model calibration began with the hydraulic properties of the calibrated steady-state model conditions and faults are absent (Table 9). Results from the transient sensitivity analysis are shown as plots of simulated values against observed values from the pressure monitoring wells. Increasing the Arbuckle hydraulic conductivity by two magnitudes from initial conditions and Arbuckle specific storage produced simulated heads closer to field-measured values in all six monitoring wells. The transient model is most sensitive to these two parameters.

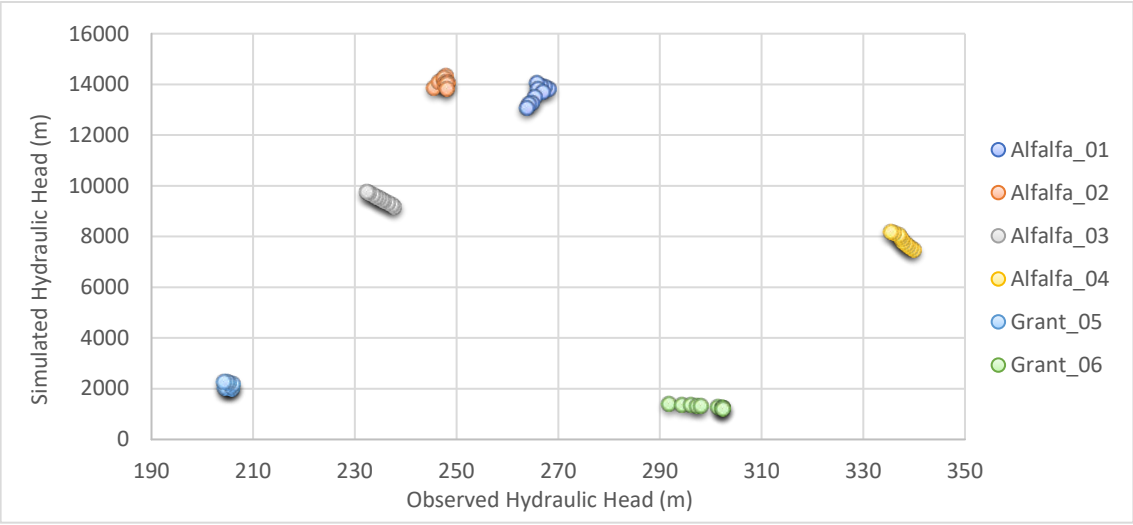


Figure 10: Observed vs simulated values for the initial parameters for the transient model acquired from the calibrated steady state model

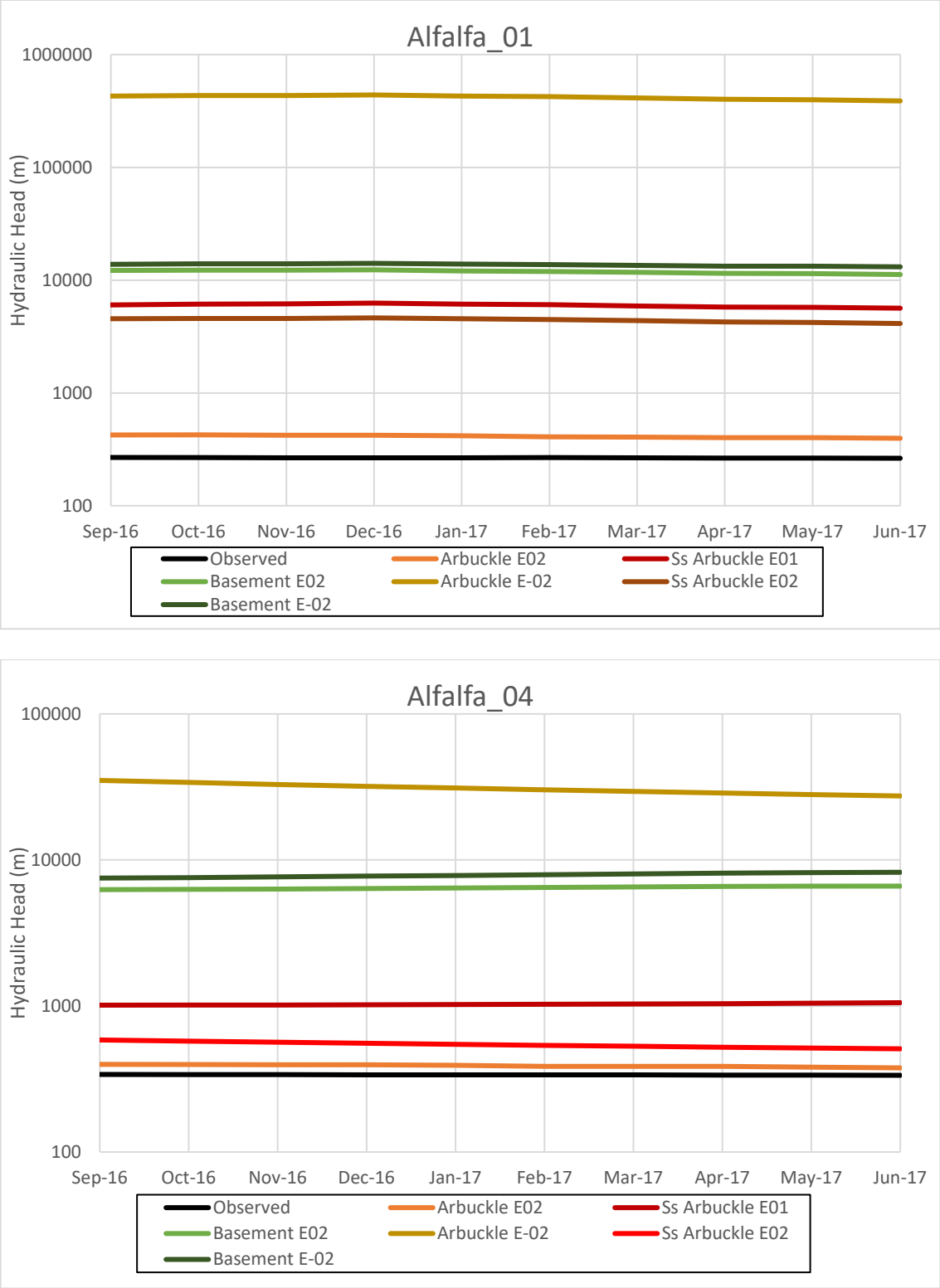


Figure 11: Pressure results for Alfalfa_01 and Alfalfa_04 from the sensitivity analysis performed on the transient model by varying parameters of the Arbuckle and Timbered Hills-Basement layer.

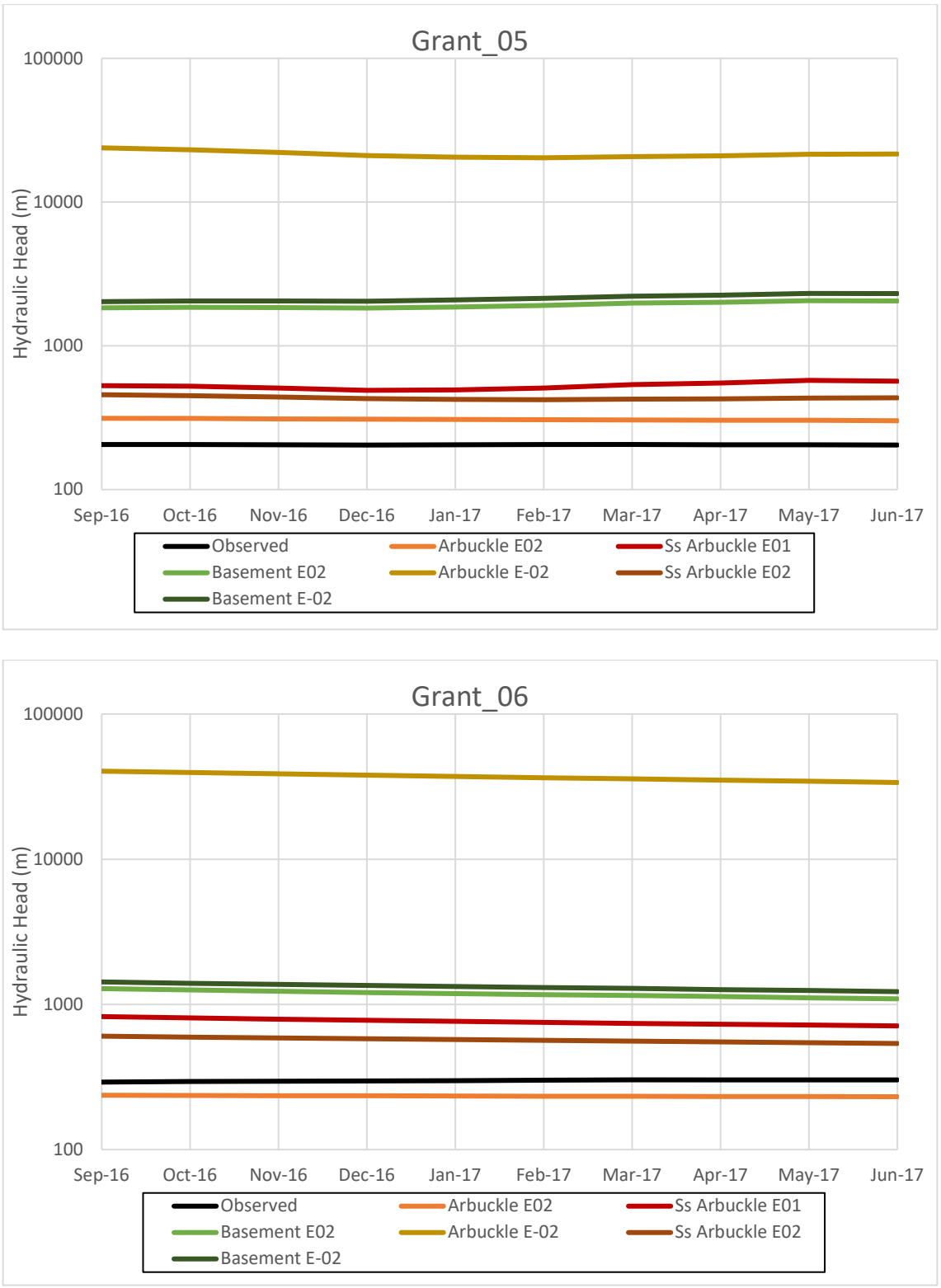


Figure 12: Pressure results for Grant_05 and Grant_06 from the sensitivity analysis performed on the transient model by varying parameters of the Arbuckle and Timbered Hills-Basement layer.

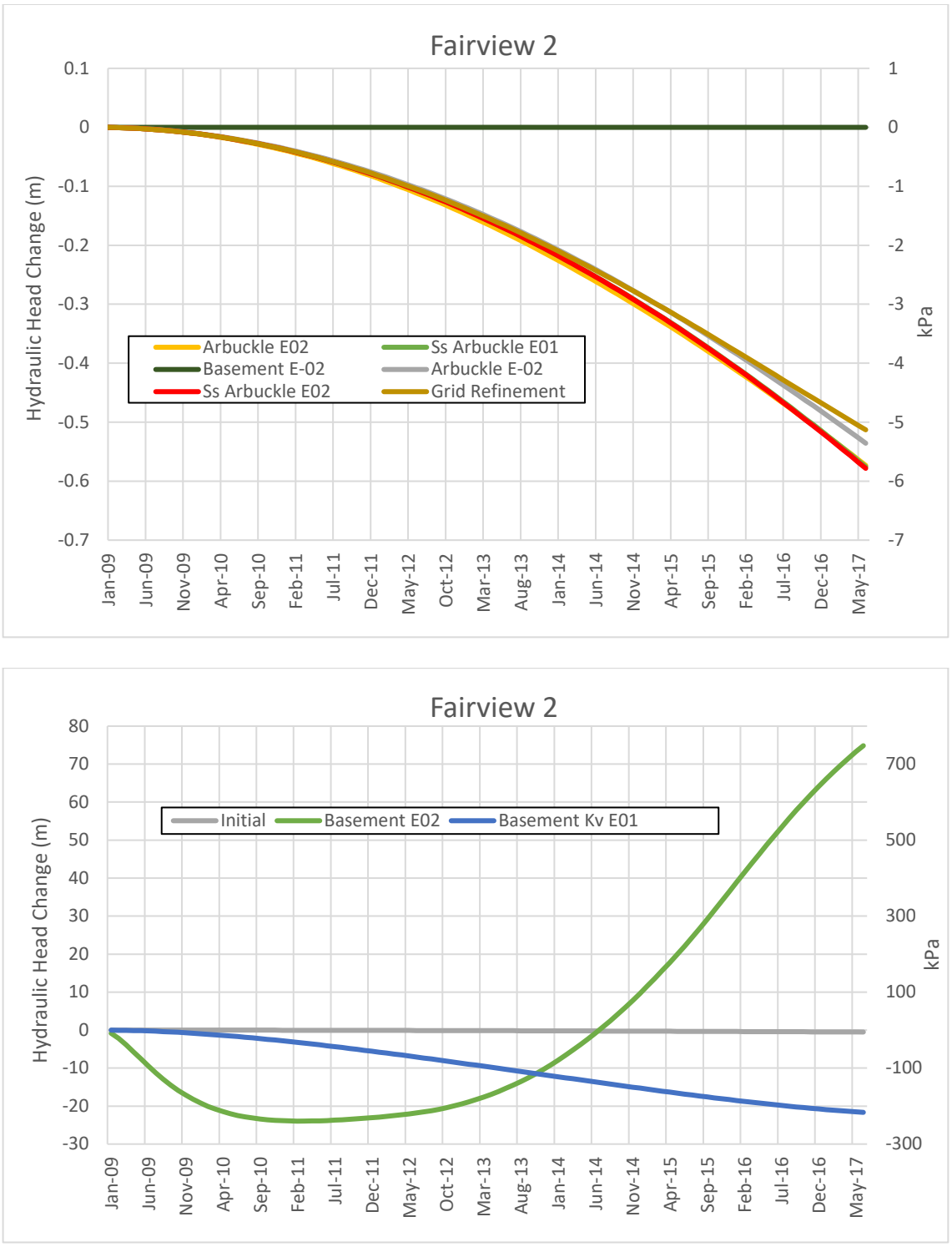


Figure 13: Pressure change computed at observation point, Fairview 2, located at a depth of 4.05 km. Pressure changes for the transient sensitivity analysis are simulated from January 2009–June 2017.

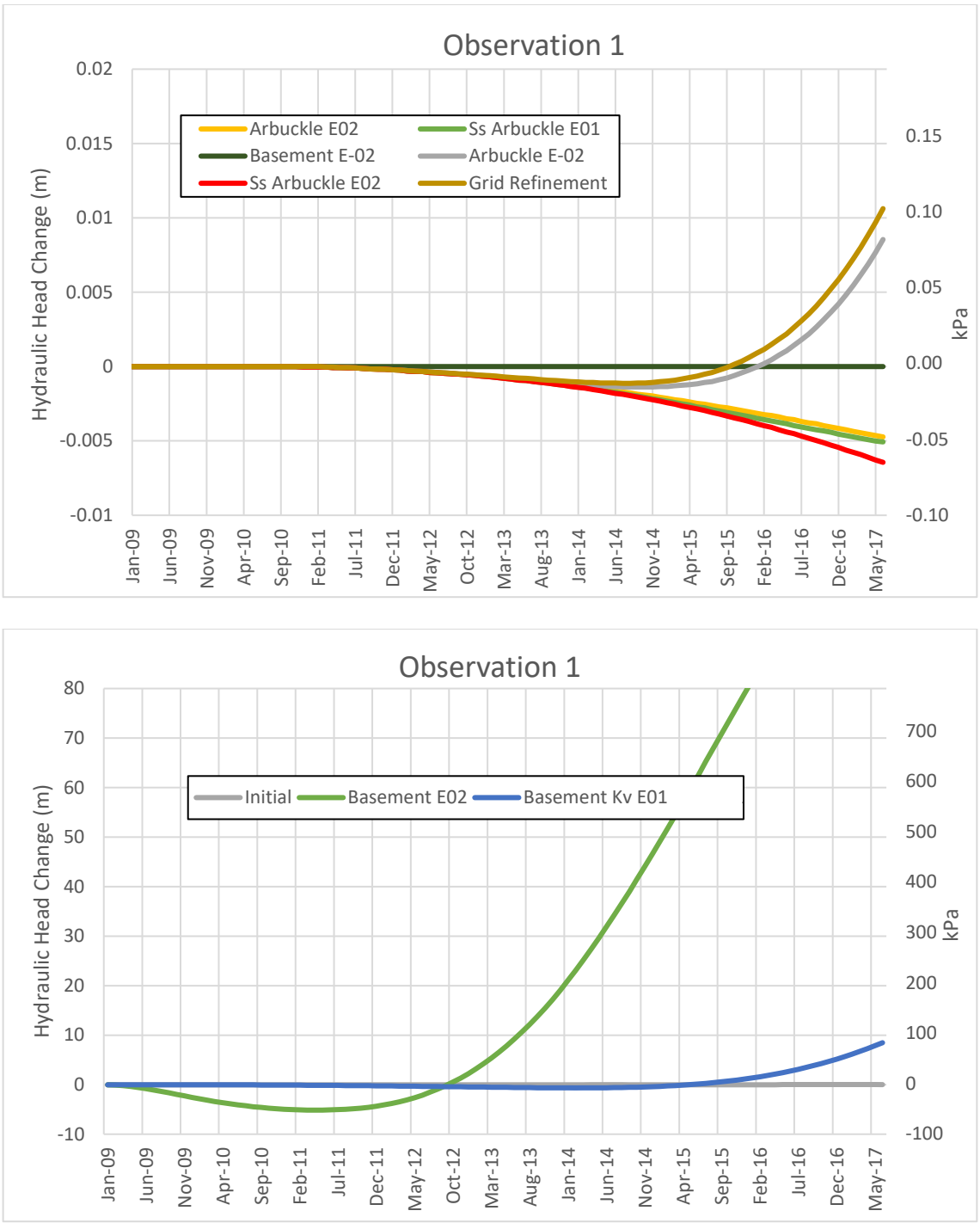


Figure 14: Pressure change at observation point, Observation 1, located about 4 km from Alfalfa_04 and Grant_05 at a depth of 4 km.

6.3.1 Scenario 1: Arbuckle Sub-layers

For transient model scenarios, hydraulic conductivity for the Arbuckle layer increases by a factor of two which lowers head values closer to observed values and matches better with K values from a modified Theis analysis of an injection test performed with a neighboring injection well to Alfalfa_02. The vertical anisotropy ratio for hydraulic conductivity of the Arbuckle remains as it was previously at two. For Scenario 1, the Arbuckle Group is no longer a homogenous geologic unit but divided into different sub-layers (Lower, Middle, Upper). The Arbuckle is identified as having reservoirs with different types of permeability within the group of formations (Scheffer, 2012). The distribution of various depositional facies resulted in a less permeable Middle Sub-layer of the Arbuckle than the Upper and Lower Sub-layers. For Scenario 1, the sub-layers of the Arbuckle are differentiated into more permeable units and less permeable units to understand how these sub-layers will affect pore-pressure propagation and changes in simulated head values. A more permeable Middle Sub-layer compared to the Upper and Lower Sub-layers will also be tested.

Initial Parameters	Post Silurian	Silurian to Middle Ordovician	Arbuckle	Timbered Hills-Basement
Kh (m/d)	3.05E-05	0.032	Varied	9.14E-04
Kv (m/d)	3.05E-13	3.05E-13	Varied	4.57E-07
Ss (1/m)	8.00E-06	8.00E-06	4.53E-07	1.00E-07
Faults	None			

Table 10: Model parameters used for the Scenario 1 of the various scenarios used to simulate the transient model.

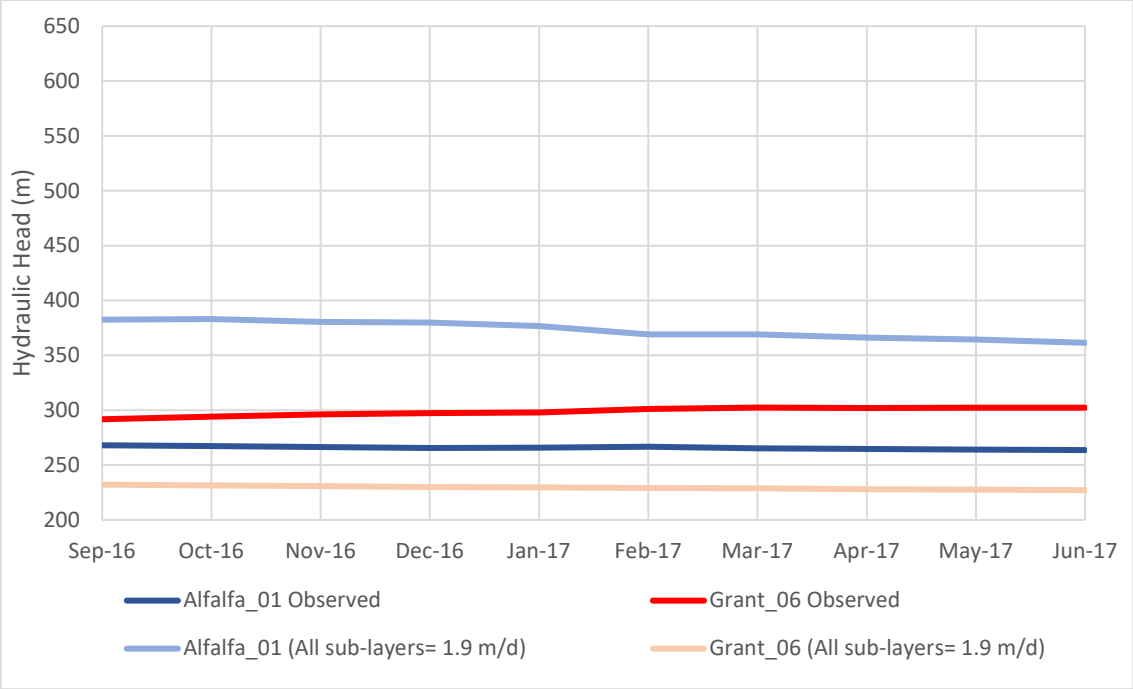


Figure 15: Simulating the resulting hydraulic head values of Alfalfa_01 and Grant_06 with uniform hydraulic conductivity values for all three sub-layers (Upper, Middle, and Lower).



Figure 16: Results of Scenario 2 varying the conductivity of each of three sub-layers of the Arbuckle layer. The top plot shows hydraulic head results of an impermeable Upper and Lower Sub-layer. The bottom diagram shows the results of a less impermeable Middle Sub-layer.

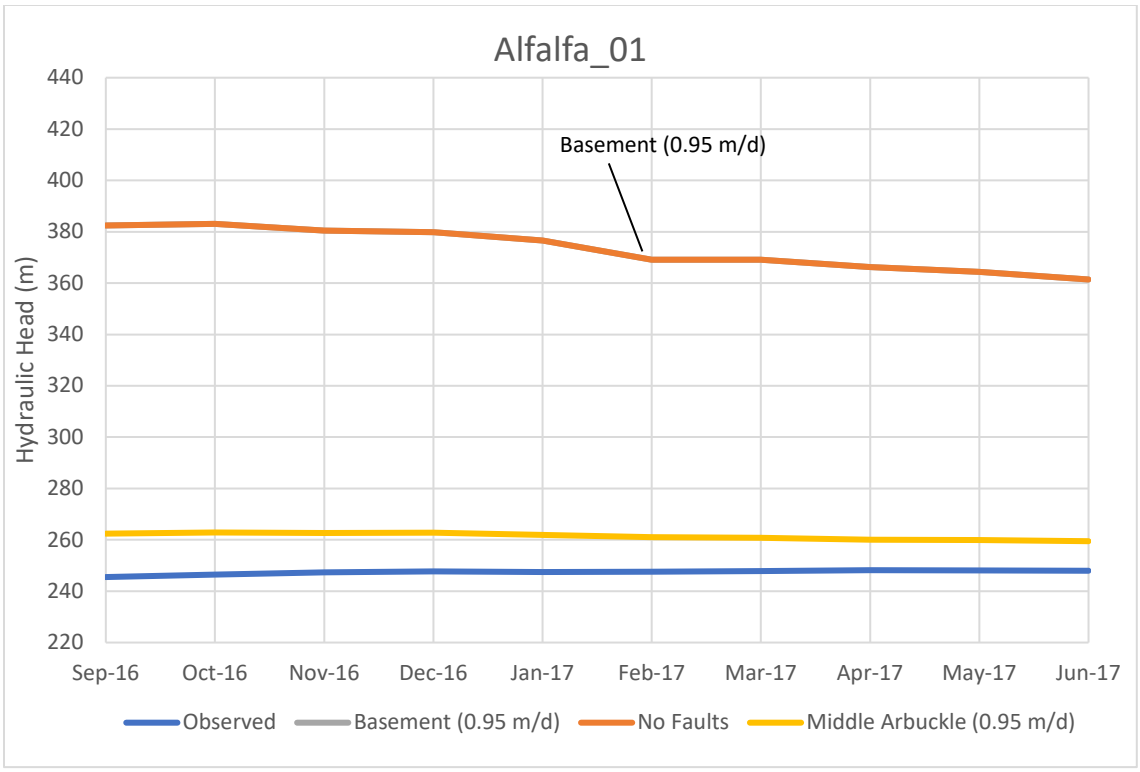
6.3.2 Scenario 2: Faults with uniform properties

For Scenario 2, faults are activated within the model domain and assigned plausible permeability values. Additionally, the faults are placed at elevations within both the Timbered Hills-Basement and Arbuckle layers. Understanding the potential conductivity of the fault zones in Oklahoma is vital to deciphering the hydraulic communication between the Arbuckle and the Timbered Hills-Basement. The ability for a fault to be a conduit for flow depends on the permeability of the fault compared to other reservoir layers (Bredehoeft et al., 1992). Initial fault permeability values are gathered from previous studies then altered during the calibration process. Carrell (2014) modeled pore-pressure changes in the Nemaha Uplift geologic province in North-central Oklahoma and used a horizontal fault hydraulic conductivity and vertical hydraulic conductivity of 9.144E-8 m/d (3.0E-7 ft/d) and 3.048E-13 m/d (1.00E-12 ft/d), respectively. Ogwari and Horton (2016) also used numerical modeling to understand pore-pressure diffusion on the Guy-Greenbrier fault in Arkansas. Using fault diffusivity and seismicity patterns, the conductance of the Guy-Greenbrier fault was calculated for the numerical model (Ogwari and Horton, 2016). With a depth decay of hydraulic conductivity, the fault section less than 5 km has a hydraulic conductivity of 0.053 m/d and the section below 5 km has a conductivity value of 0.024 m/d (Ogwari and Horton, 2016). Other studies analyzing injection-induced seismicity in the Midcontinent region assigned basement faults permeability values ranging from 1E-12 m^2 to 1E-15 m^2, hydraulic conductivity values 1.2 m/d and 0.0012 m/d, respectively (Zhang et al., 2013). Studies in Texas on the equivalent strata to the Arbuckle (the Ellenburger formation) modeled pore-pressure diffusion on faults extending into the shallower Ellenburger formation (Hornbach et al., 2015), and assigned fault permeability 50% lower than the Ellenburger Formation, values used between 1.5E-15 m^2 and 0.5E-13 m^2.

If fault elevation is only assigned to the Timbered Hills-Basement layer for the model, not enough pressure is able to diffuse from injection wells in the Arbuckle layer to lower hydraulic head values in pressure-monitoring wells. Other studies model faults in both the Arbuckle Group and basement rock and confirm the highly complex permeability of limestone faults and fracture/damage zones (Hornback et al., 2015). The lower z-coordinate of all mapped faults within the model domain is in the Timbered Hills-Basement layer. Scenario 2 simulated pressure results of faults extended into the Lower Arbuckle Sub-layer, Middle Arbuckle Sub-layer, and Upper Arbuckle Sub-layer from the basement. Further discretizing the Arbuckle layer into three sub-layers, provided a better resolution of data and the opportunity to investigate the heterogeneity of the unit.

Initial Parameters	**Post Silurian**	**Silurian to Middle Ordovician**	**Arbuckle**	**Timbered Hills-Basement**
Kh (m/d)	3.05E-05	0.032	1.9	9.14E-04
Kv (m/d)	3.05E-13	3.05E-13	0.277	4.57E-07
Ss (1/m)	8.00E-06	8.00E-06	4.53E-07	1.00E-07
Faults	Uniform properties/various elevations			

Table 11: Model parameters used for transient model to run Scenario 2 and observe head changes within monitoring wells.



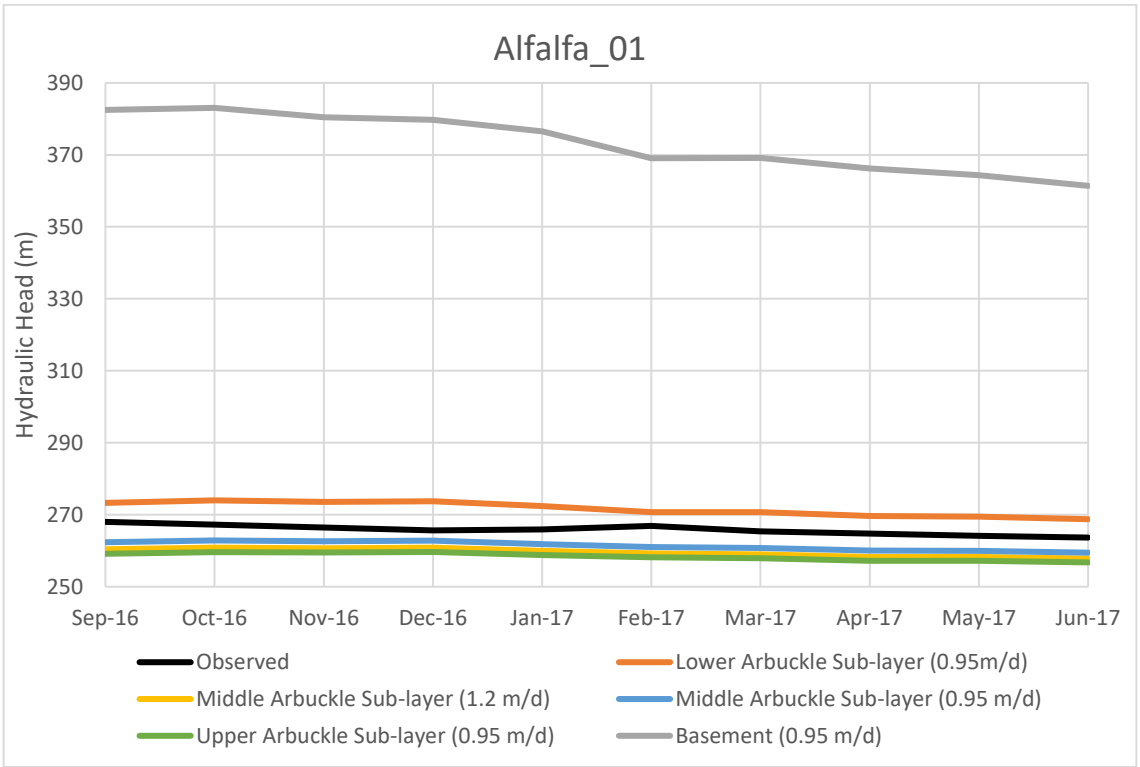


Figure 17: Top diagram shows pressure changes in Alfalfa_01 with the presence of faults. The bottom plot shows previously mapped faults within the model domain with uniform permeability at different elevations.

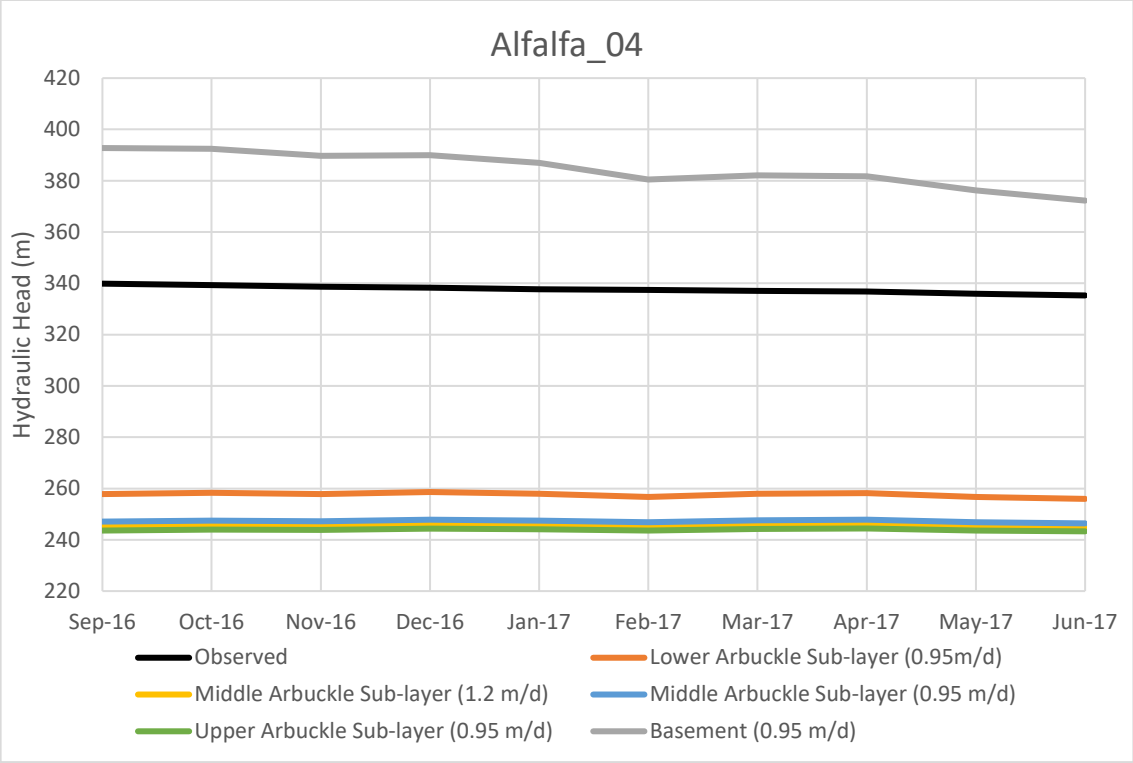
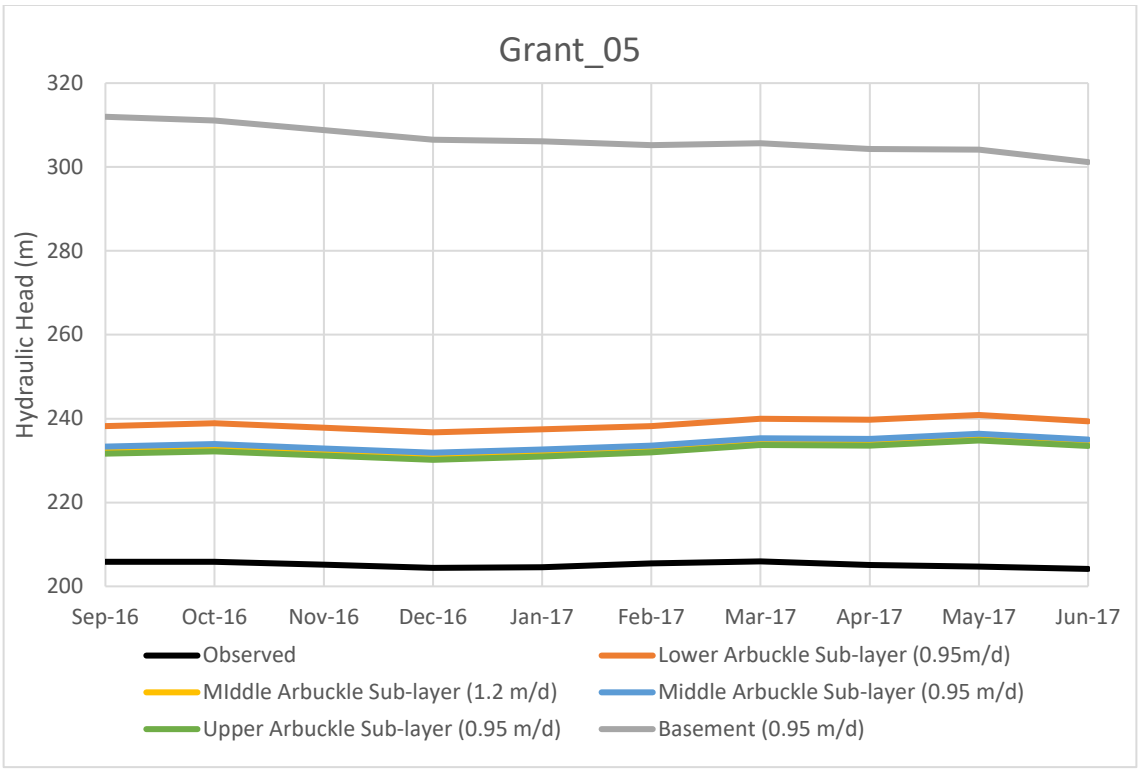


Figure 18: Results of Scenario 2 for the transient model and the head values simulated in Alfalfa_04.



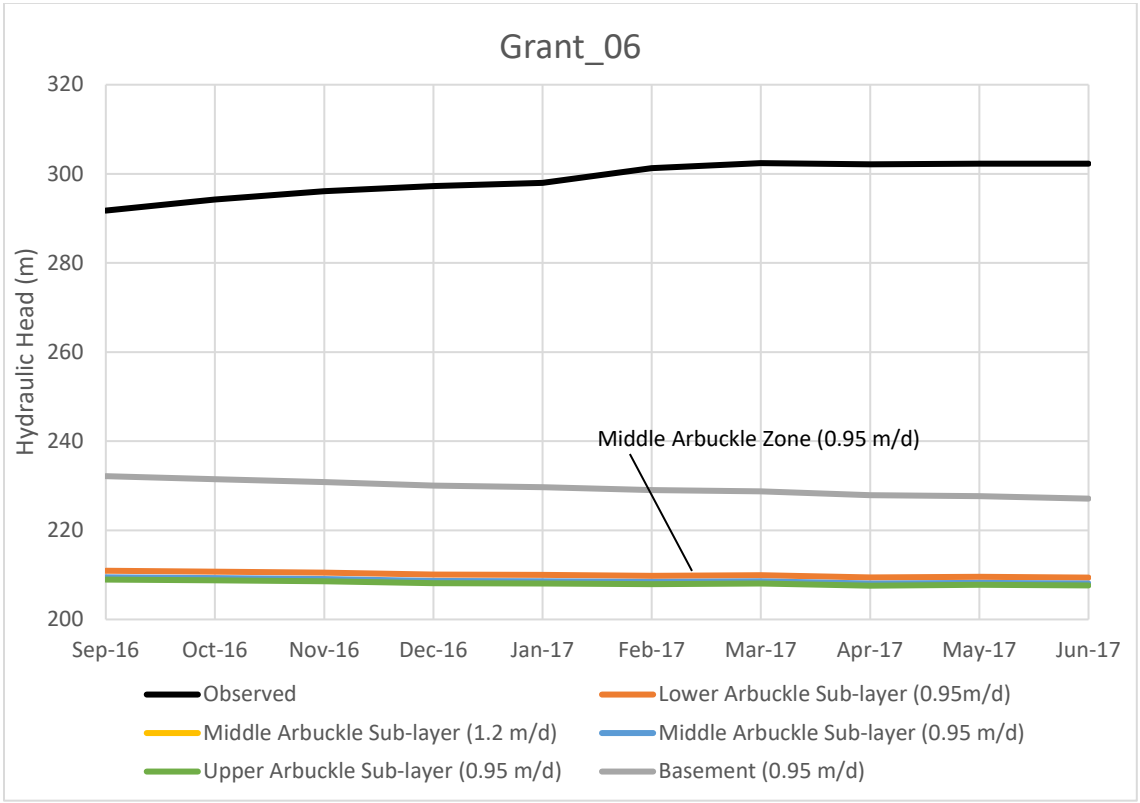


Figure 19: Results of uniform fault permeability at different elevations within the Arbuckle layer for Grant_05 and Grant_06.

6.3.4 Scenario 3: Varying fault properties

Analyzing the results of the sensitivity analysis and scenarios for the transient model, simulated and observed head values in the monitoring wells continued to have a large discrepancy. The simulated head values for multiple Alfalfa wells remained too high while head values for Grant_06 were substantially lower than observed values. Instead of assigning uniform properties to all mapped faults within the model domain, Scenario 3 approach faults individually and assigned properties deemed appropriate. Mapped faults around Alfalfa_01, Alfalfa_02, Alfalfa_03 were assigned to be conductive (0.95 m/d) and impermeable near Alfalfa_04. Dividing the Arbuckle into three sub-layers, the elevation of the faults was assigned to the Lower Arbuckle Sub-layer. When the conceptual model was created, the Arbuckle layer was lowered 500 m to accommodate the depths of injection recorded on SWD well logs. This action increased the depth to the top of the Timbered Hills-Basement layer and increased the thickness of the Arbuckle layer. The results of Scenario 3 for this scenario remain unsuccessful in decreasing the head residual.

Initial Parameters	**Post Silurian**	**Silurian to Middle Ordovician**	**Arbuckle**	**Timbered Hills-Basement**
Kh (m/d)	3.05E-05	0.032	1.9	9.14E-04
Kv (m/d)	3.05E-13	3.05E-13	0.277	4.57E-07
Ss (1/m)	8.00E-06	8.00E-06	4.53E-07	1.00E-07
Faults	Various properties/uniform elevation			

Table 12: Initial parameters used for Scenario 3 of the transient model simulations.

6.3.5 Inferred Faults

Without a large correlation between earthquake epicenters and mapped faults, studies have investigated potential fault locations using focal mechanism solutions and wellbore

breakout stress orientations (Alt and Zoback, 2017). Five “inferred” fault fragments are placed in the model domain for this study. Although earthquake scaling laws confirm large magnitude earthquakes occur on deep faults, the structure of both the Arbuckle and basement are heterogenous and poorly understood. Figure 11 shows the distribution of earthquakes above the depth of 4 km in the study area of the model. Within the model domain, two permeable fault segments were placed near Alfalfa_02 and Alfalfa_03, one near Grant_05, and two impermeable faults near Grant_06 (Figure 14).

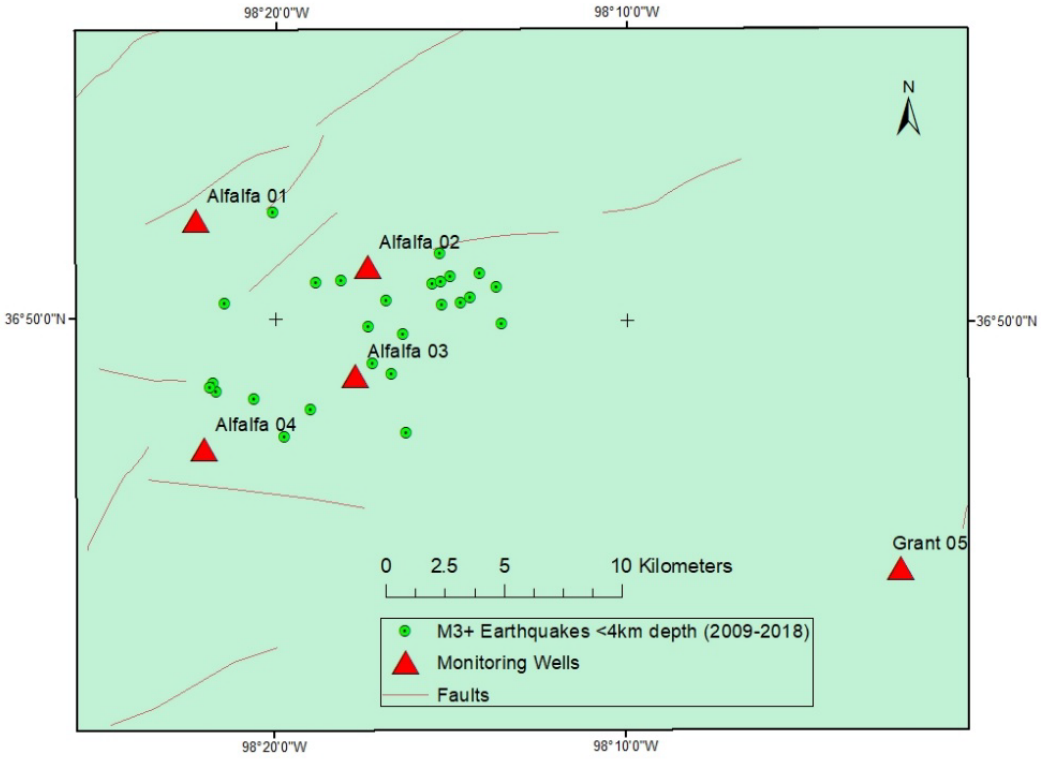


Figure 20: Map of study area showing shallow earthquakes around Alfalfa_02 and Alfalfa_03 less than 4 km in depth.

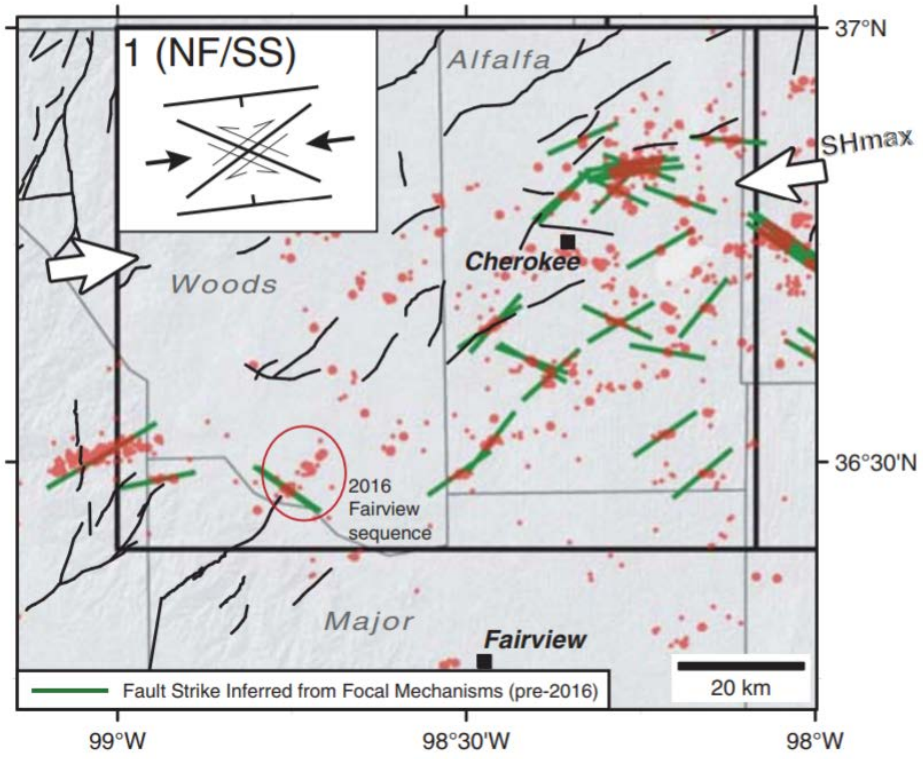


Figure 21: A map of the study area produced by Alt and Zoback (2017) to show fault planes (green lines) assumed to have slipped to produce the earthquakes events shown as red dots. These "inferred" faults were mapped using available focal mechanism solutions and stress orientations from wellbore hole data (Alt and Zoback, 2107). The black lines represent previously cataloged faults.

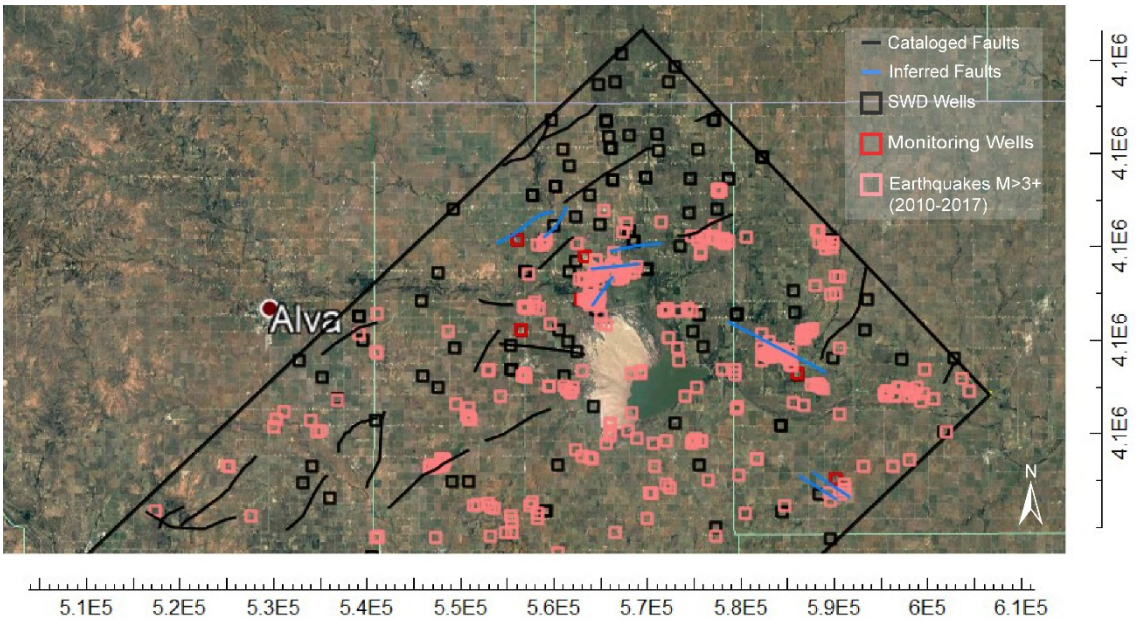


Figure 22: ModelMuse image of inferred faults placed in the model domain assigned a hydraulic conductivity of 0.95 m/d.

6.4 Evaluation of Model Calibration/Measures of Error

Evaluating the model fit for a numerical groundwater flow model involves quantifying the quality of model calibration. The calibration criterion for this study aims to match simulated hydraulic head values to the observed field-measured hydraulic head values from monitoring wells. The difference between observed and simulated head values is the residual (Anderson and Woessner, 1992). Measures of error rooted in statistical methods are used to quantify the error between head values during the calibration process. An acceptable range of error depends on the spatial scale and goals of the model. The measure of error used to evaluate the model calibration for this study is the mean square root of the residuals (Reilly and Harbaugh, 2004). The error criterion used in this study represents the average error in the calibrated model, and the spatial distribution of error was qualitatively evaluated from plotted head residuals for each monitoring well (Anderson and Woessner, 1992). Once the model reached calibration, an additional sensitivity analysis was conducted (Figure 25).

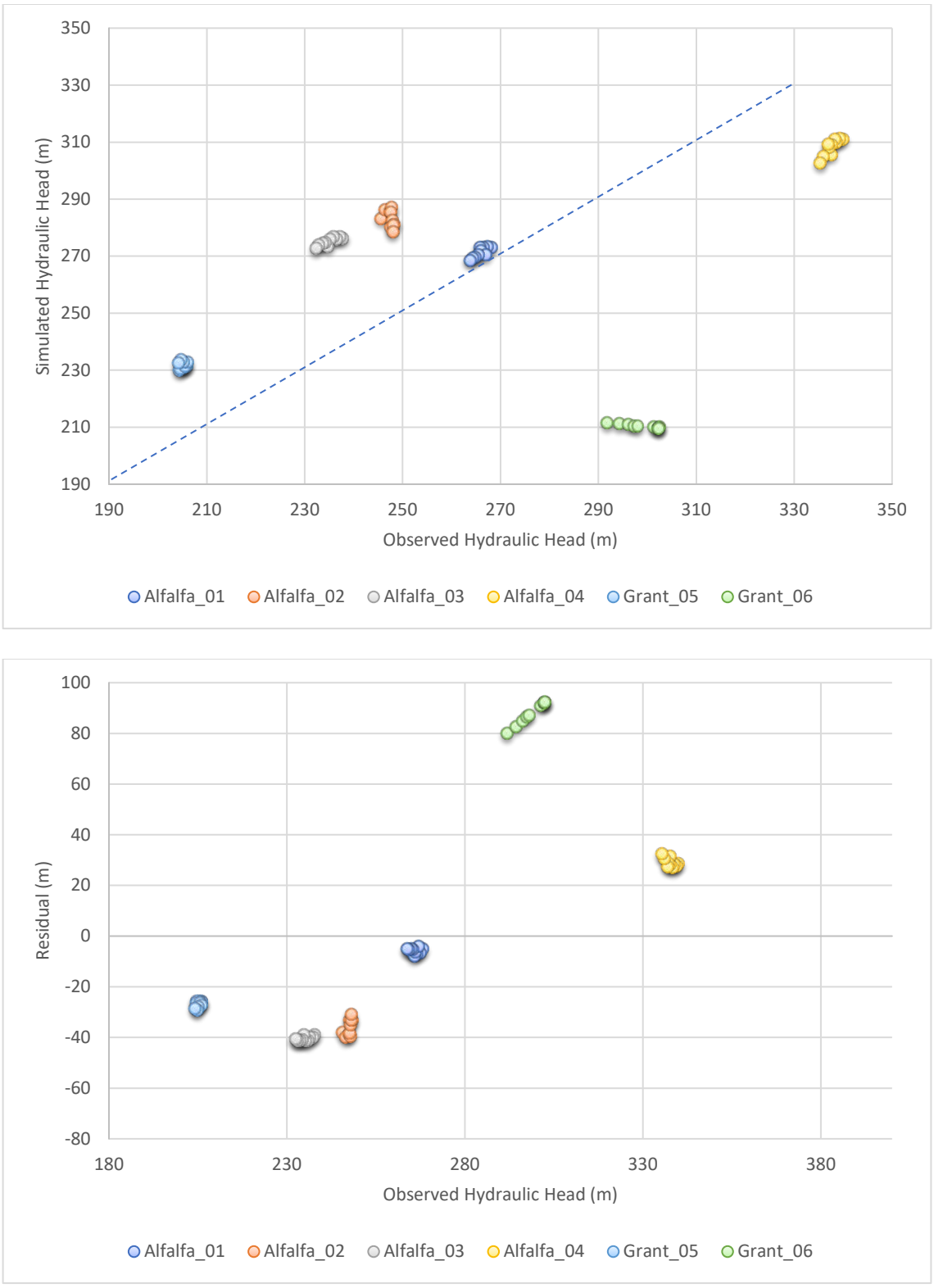
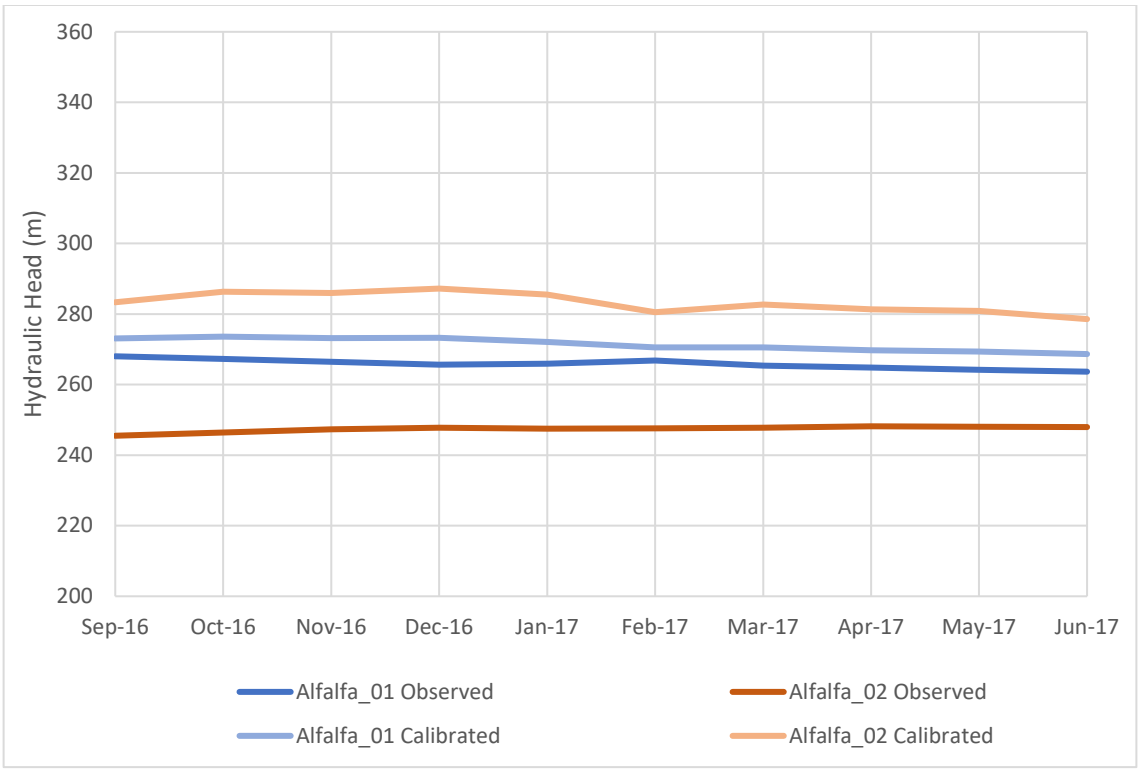


Figure 23: Observed/simulated values and head residuals plotted for the six monitoring wells during calibration (September 2016–July 2017). If there is a perfect match, then head values would be aligned along the dotted line.



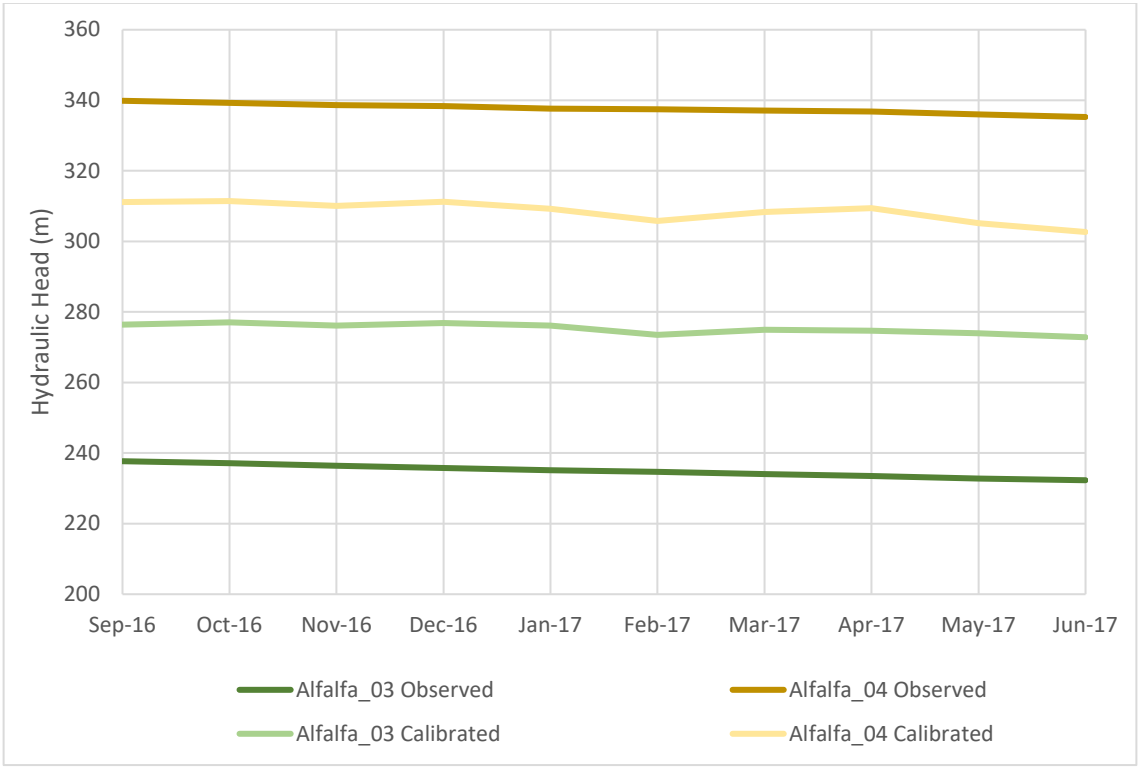


Figure 24: Change in observed vs simulated head pressure values (m) in Alfalfa_03 and Alfalfa_04 values for final calibrated model.

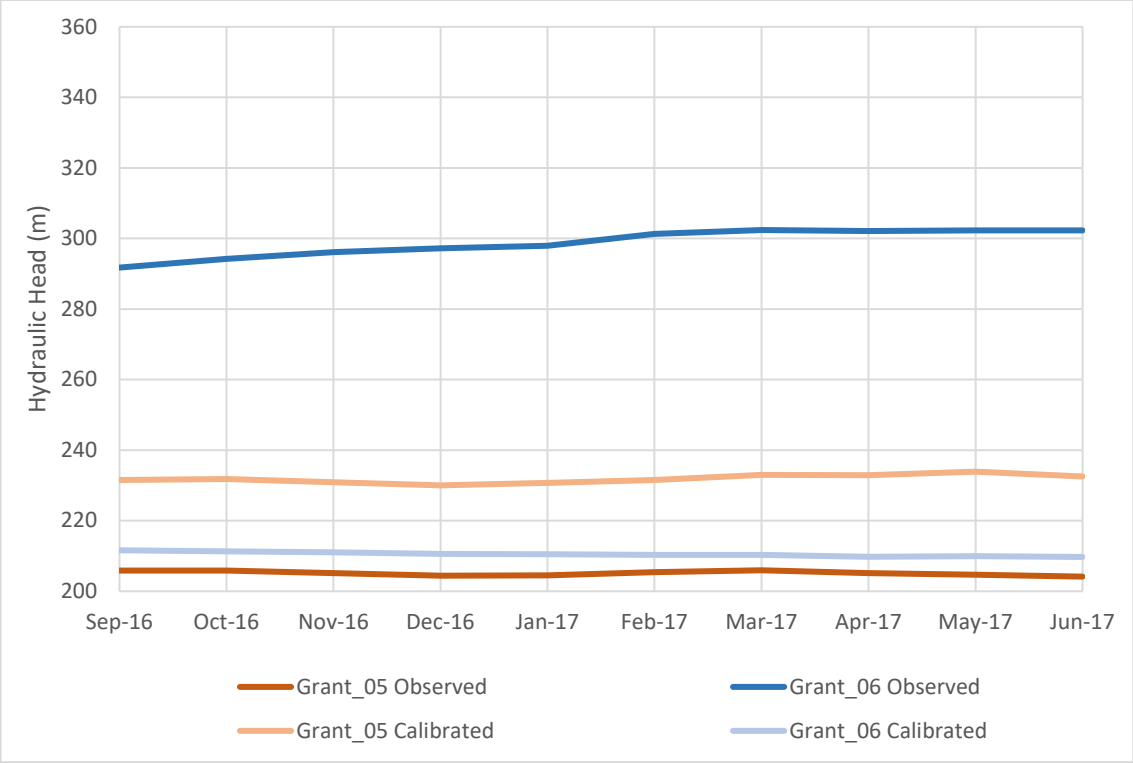


Figure 25: Change in observed vs simulated head pressure values (m) in Grant_05 and Grant_06 values for final calibrated model.

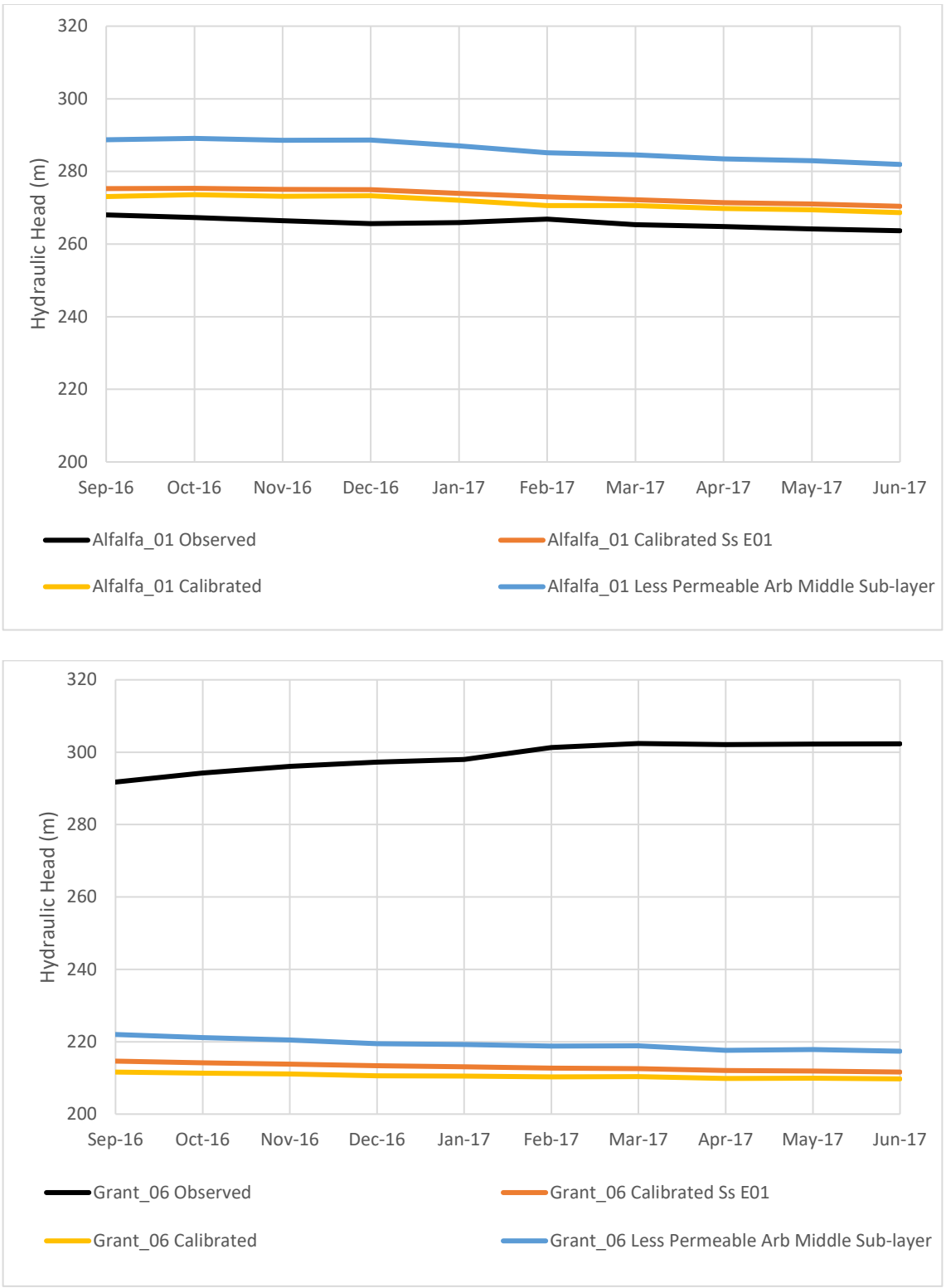


Figure 26: Sensitivity analysis performed on the calibrated transient model. Hydraulic head results for Alfalfa_01 and Grant_06.

Although the calibration process minimizes uncertainty and error, the calibrated model may still contain inaccuracies in representing the true field parameters of the system (Anderson and Woessner, 1992). The model is validated by using the calibrated model to simulate a new time period for which observations are available and comparing simulated versus observed heads. The model in this study is calibrated against data from September 2016–June 2017 (10 months) and validated for July 2017–April 2018 (10 months).

The finial calibrated model has a mean square root residual of 29.83 m. Qualitatively, the spatial distribution of error is analyzed by identifying the magnitude of head residual for each well. Alfala_01 has the smallest head residual of -5.59 m for the average of 10 months while Grant_06 has the largest with an average of 88 m., but a measure of error should not be the sole measure of model accuracy. A conceptually sound model is superior to a model that has perfectly matched observed to simulated heads (Reilly and Harbaugh, 2004).

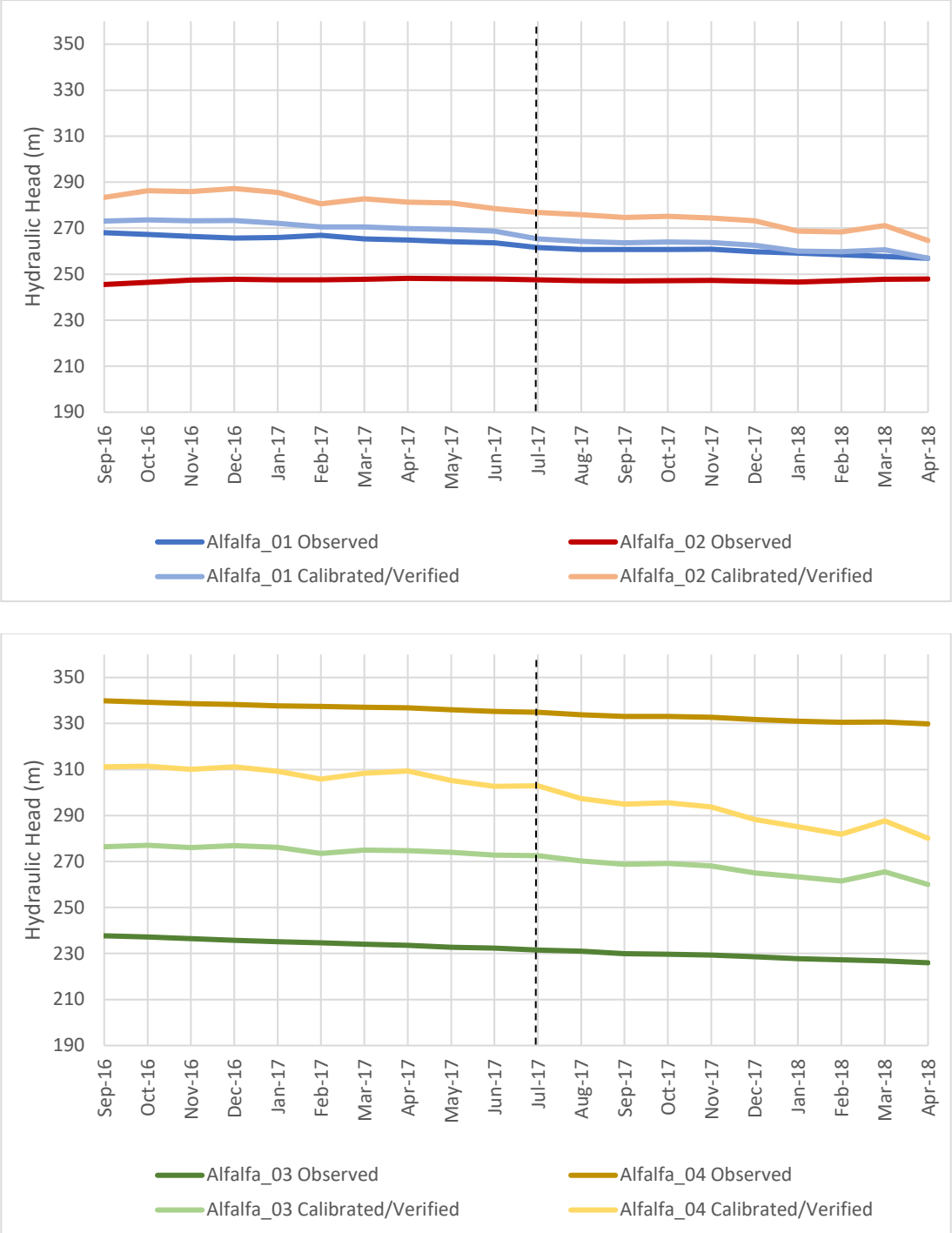


Figure 27: Calibrated (September 2016–June 2017) and validated (July 2017–April 2018) head values for monitoring wells located in Alfalfa County.

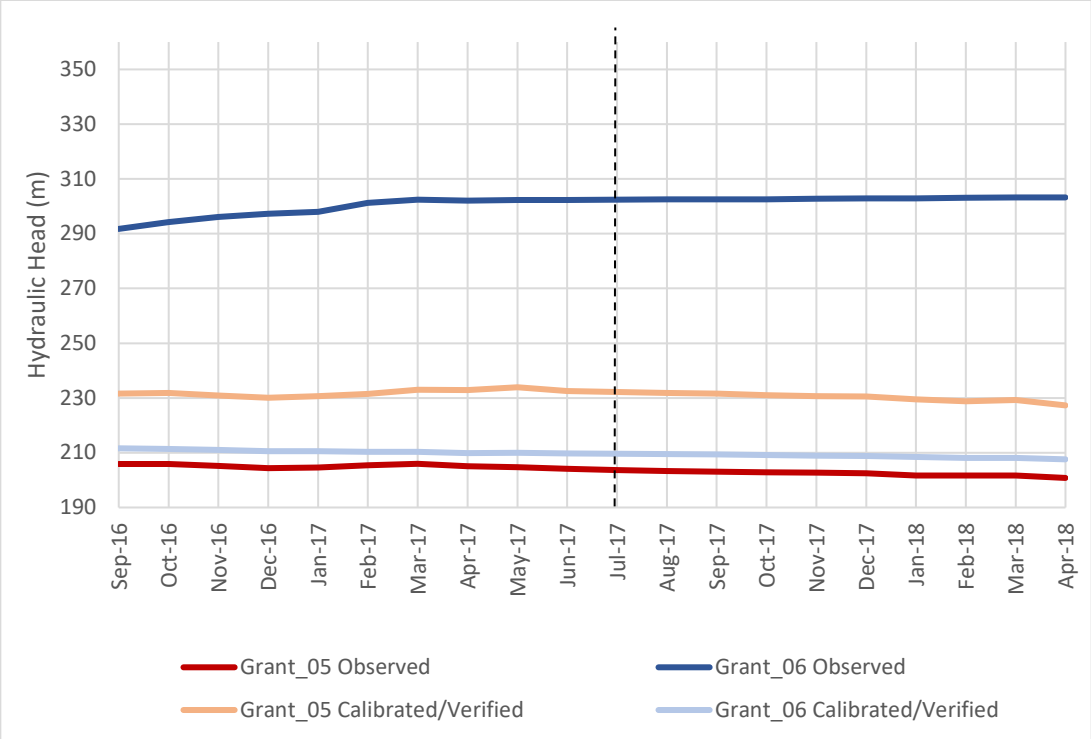


Figure 28: Calibrated (September 2016–June 2017) and validated (July 2017–April 2018) head values for monitoring wells located in Grant County.

Chapter 7: Discussion

Numerous studies conclude that conductive faults and fracture zones can highly influence pore-pressure diffusion (Hsieh and Bredehoeft, 1981; Ogwari and Horton 2016, do Nascimento et al., 2004; and Zhang et al., 2013). This study strongly suggests similar fault/fracture zone behaviors in north-central Oklahoma to accommodate wastewater injection. This study also confirms the spatial heterogeneity of fault properties (i.e. permeability) at a regional scale. Limestone fracture zones are highly heterogenous and likely influencing pore-pressure development at the fault and within the surrounding geologic units (Hornbach et al., 2015). The fault permeability resolved for the calibrated model of this study is 6.627E-13 m^2 which agrees with fault properties in similar studies of induced seismicity in the Midcontinent (Zhang et al., 2013; and Hornbach et al., 2015).

Far-field pressurization is a suggested mechanism for the Fairview earthquake sequence (Yeck et al., 2017). The earthquake sequence occurs more than 20 km from a cluster of high-rate injection wells located northeast of the Fairview fault. Peak injection does occur prior to the rapid increase indicating that pore pressure is a prominent mechanism for the Fairview seismicity (do Nascimento et al., 2004). For the combined 113 SWD wells in the study area, total monthly volumes increase from 1.5 Mbbls in January 2009 and peak around 30 Mbbls in March 2015.

Previous numerical modeling studies for the Fairview earthquake sequence computed a pressure change ranging from 0.003–0.100 MPa (3–100 kPa) around the Fairview region at 3 km depth (Goebel et al., 2017). Results from this study compute almost negligible pore-pressure changes at observation points located at the Fairview earthquake hypocenters (Fairview Main/ 8 km, Fairview 2/ 4 km) unless the hydraulic conductivity of the Timbered Hills-Basement layer is increased by two orders of magnitude (4.47E-02 m/d), which is unrealistic for granitic rock (Figure 12). Pressure changes simulated at a depth of 3 km in the Fairview region, Observation 2, show pressure changes within the range previously stated from Goebel et al. (2017) (Figure 28). Observation 2 is located within the Lower Arbuckle Sub-layer, not the Timbered Hills-Basement layer. Additionally, pressure changes were computed at Observation 2 with the hypothetical situation of all faults within the model domain acting as conduits for flow (Figure 29). Comparing the results of Figure 28 and Figure 29, pressure changes are smaller at the Fairview region when all faults are active, confirming their role in propagating pore-pressure effectively from SWD wells. Similar pore-pressure decreases are simulated in the Fairview region when the 14-km long Fairview fault is hypothetically extended to the cluster of SWD wells in the Fairview region (Goebel et al., 2017). Studies suggest poroelastic effects play a role in the Fairview seismicity (Goebel et al., 2017). A coulomb stress change of 0.4 MPa (400 kPa)

is needed to induce the large magnitude (M 5.1) earthquake recorded in Fairview, OK, and pore pressure alone may not be able to produce this stress change (Yeck et al., 2017).

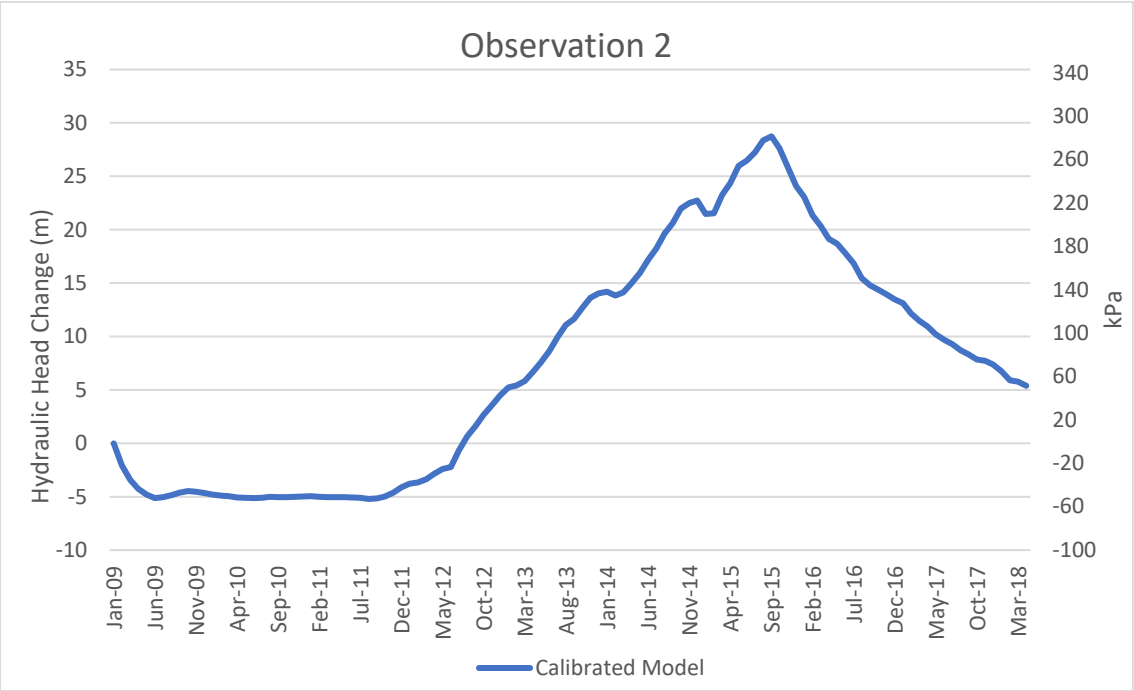


Figure 29: Observation 2 is an observation point located near the Fairview earthquake sequence. Pressure changes are recorded at 3 km for the entire duration of the model (January 2009–April 2018).

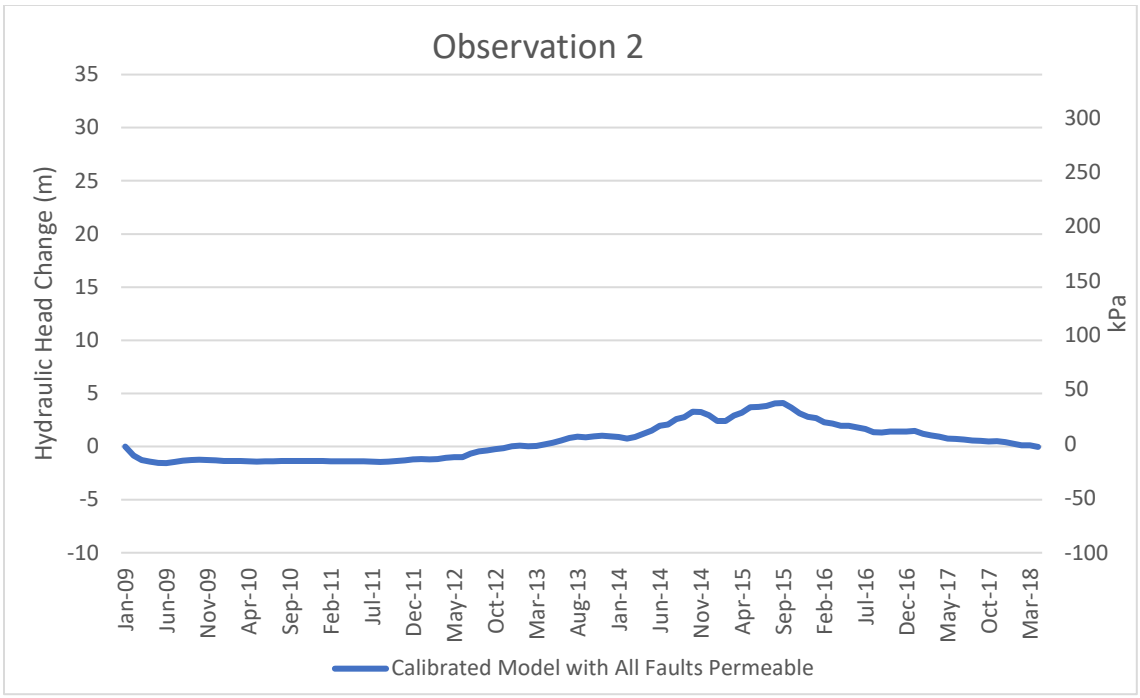


Figure 30: Smaller pressure changes are computed at Observation 2 when all faults within the model are permeable. Figure 29 shows pressure changes for the calibrated model which assigns faults as both permeable and impermeable.

Chapter 8: Conclusions and Future Work

8.1 Conclusions

Before simulating pressure changes at observation points, the model underwent an extensive calibration process. The best-fit model was measured against an error criterion that aimed to achieve the smallest root mean squared head residual for all six monitoring wells. Sensitivity analyses were conducted on both steady-state and transient models to achieve the best-fit model, and properties for the Arbuckle were resolved that differ from previous studies (Carrell, 2014; Ogwari and Horton, 2016; Perilla, 2017; and Williams, 2017). From matching simulated to observed heads using the MODFLOW model, the best-fit hydraulic conductivity (1.9 m/d) and specific storage (4.53E-07 m^{-1}) must be increased by one to two orders of magnitude above previously published values.

As previously stated, this study supports the role geological structures play in propagating pore-pressure from SWD wells. Model calibration was achieved once faults within the model domain were made conductive. Moreover, additional faults were placed in areas of high-pressure to aid in reducing the head residual in each monitoring well. A fault zone of higher vertical conductivity must be present near Alfalfa_02 and Alfalfa_03 to fit simulated heads to observed heads. Overall, the Alfalfa monitoring wells show a smaller head residual than the Grant wells. A head residual of -5 m is computed for Alfalfa_01, while Grant_06 has an average 80 m head difference.

	Initial head (m)	Observed head (m) 4/2018	Simulated head (m) 4/2018
A01	243.28	256.91	256.94
A02	241.94	247.96	264.61
A03	238.50	225.98	260.00
A04	235.62	329.83	280.11
G05	219.04	200.79	227.29
G06	200.17	303.20	207.59

Table 13: Initial heads for each of the monitoring wells from Puckette (1996) used to calibrate the steady-state model compared to observed values from April 2018 and simulated values for April 2018.

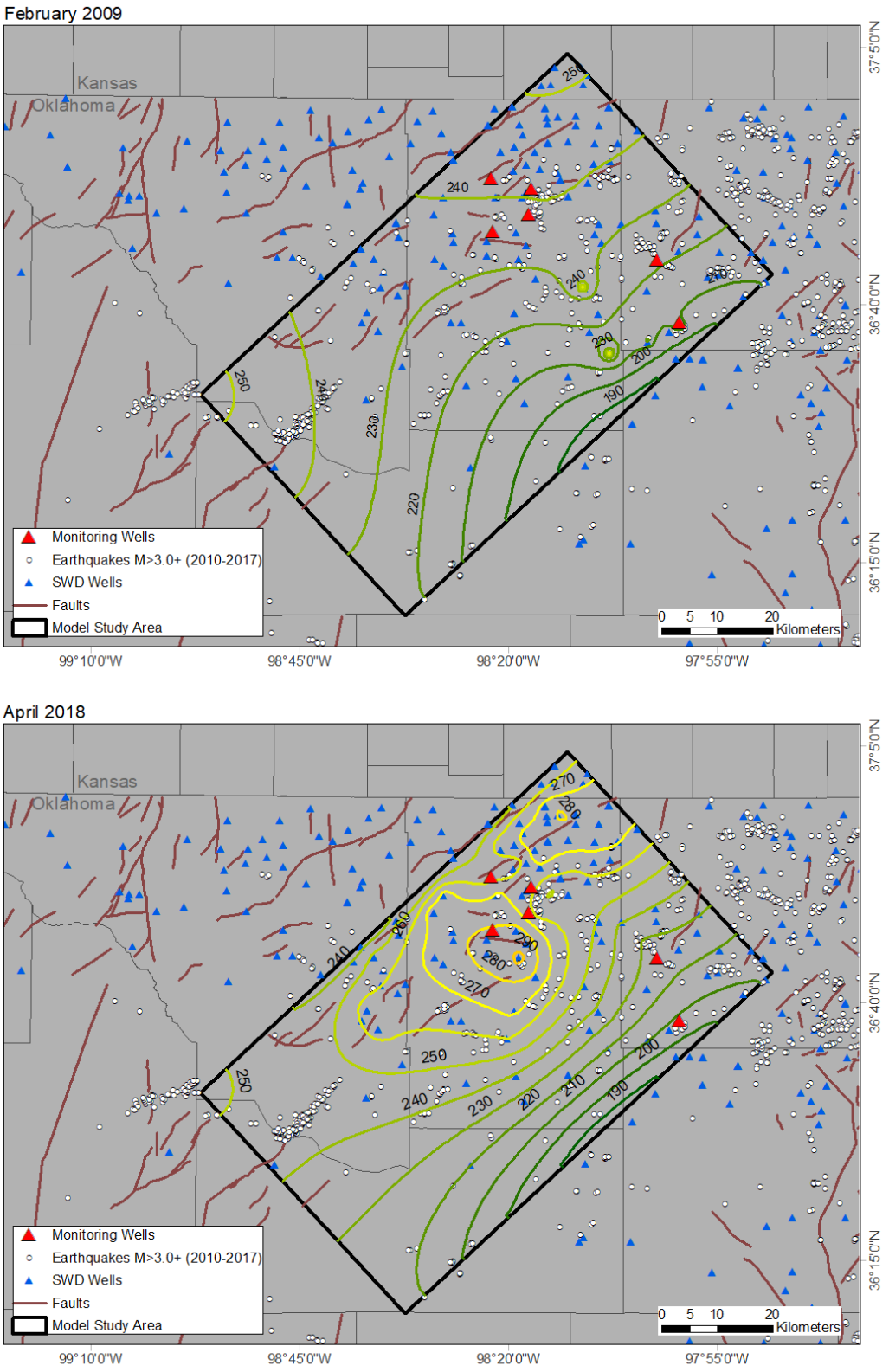


Figure 31: Potentiometric surface map showing hydraulic heads (m) one month/ time step in the transient simulation (February 2009) and after 112 months /time steps (April 2018).

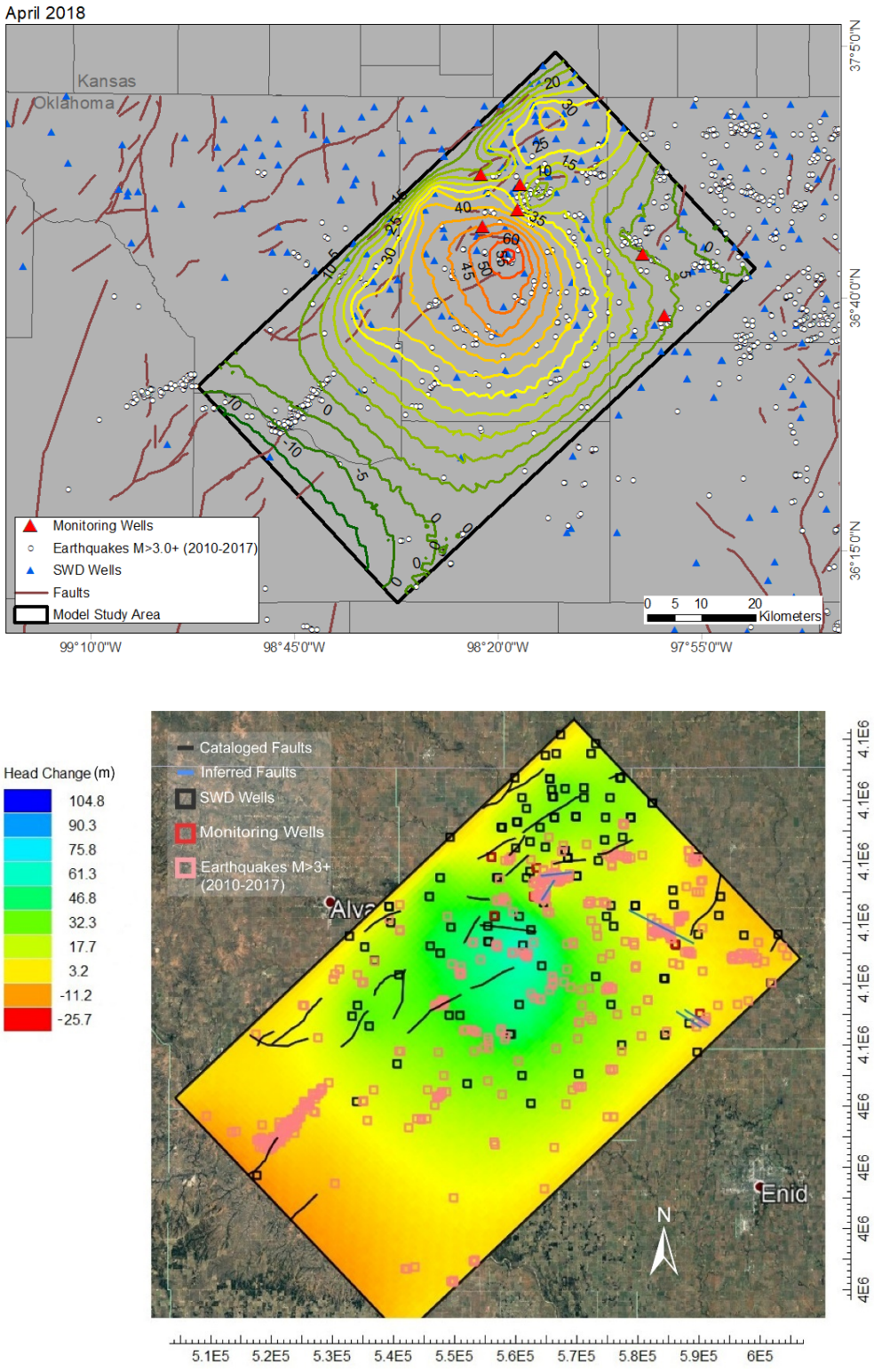


Figure 32: Total head change (m) for the Arbuckle and TH-B layer after 112 months/time steps, represented by a color grid and contours. The distance between the largest increase in head change to zero head change is 45 km.

8.2 Future Work

Two monitoring wells in Table 13 show a decrease in pressure from initial head values (1996) to observed head values (2018). Head values in monitoring wells are expected to increase not decrease after 10 years of injection. An avenue of future research would be to re-evaluate the "virgin" pressure for the Arbuckle Group that were used as starting head values for this study (Puckette, 1996). Multiple methods should be utilized to understand the initial pressure head of the Arbuckle Group before subsurface injection began for Oklahoma.

The large head residual for Grant_06 (80 m) supports a hypothesis that lateral variations in Arbuckle hydraulic conductivity exist. With additional field data to recognize heterogeneities of hydraulic conductivity within the Arbuckle Group, the model error can be further reduced. For this study, the Arbuckle was assumed to be laterally homogenous.

Other sources of error for the model in this study may be reduced by adjusting the original conceptual model in the study area. A smaller model domain and redefined boundary conditions would create a refined model with less uncertainty. Continued efforts to characterize the basement rock and faults/fracture zones of Oklahoma will greatly benefit future hydrogeological, geomechanical, or seismological models that depend on reasonable rock properties. A well constrained model of the subsurface can ultimately be used as a decision-support tool for mitigating seismicity.

References

Alt, R.C., and Zoback, M.D. 2017. In situ stress and active faulting in Oklahoma. *Bulletin of the Seismological Society of America*, 107: 1.

Barbour, A.J., Norbeck, J.H., and Rubinstein, J.L. 2017. The effects of varying injection rates in Osage County, Oklahoma, on the 2016 Mw 5.8 Pawnee Earthquake. *Seismological Research Letters*, 88: 4, p. 1040-1053.

Barnes, C., and Halihan, T. 2018. The availability of hydrogeologic data associated with areas identified by the US Geological Survey as experiencing potentially induced seismicity resulting from subsurface injection. *Hydrogeology Journal*, 26, p. 743-754

Batzle, M., and Wang, Z. 1992. Seismic properties of pore fluids. *Geophysics*, 57:11, p. 1396-1408.

Blondes, M.S., Gans, K.D., Engle, M.A., Kharaka, Y.K., Reidy, M.E., Saraswathula, V., Thordsen, J.J., Rowan, E.L., and Morrissey, E.A. 2017. U.S. Geological Survey National Produced Waters Geochemical Database v2.3. https://eerscmap.usgs.gov/pwapp/

Bredehoeft, J.D., Belitz, K., and Hansen-Sharp, S. 1992. The Hydrodynamics of the Big Horn Basin: A Study of the Role of Faults. The American Association of Petroleum Geologists Bulletin. 76, 4, p. 530-546

Carrell, Jordan. 2014. *Field-Scale Hydrogeologic Modeling of Water Injection into the Arbuckle Zone of the Midcontinent* (Master's thesis).

Crain, K.D. and Chang, J.C. 2018. Elevation Map of the Top of the Crystalline Basement in Oklahoma and Surrounding States. Oklahoma Geological Survey Open-File Report 1-2018, 3 pp.

Carr, J.E., McGovern, H.E., Gogel, T., and Doveton, J.H. 1986. Geohydrology of and potential for fluid disposal in the Arbuckle Aquifer in Kansas: U.S. Geological Survey Open-File Report (86-491), 101 pp.

Christenson, S., Osborn, N. I., Neel, C. R., Faith, J. R., Bloom, C. D., Puckette, J., and Pantea, M. P. 2011. Hydrogeology and Simulation of Groundwater Flow in the Arbuckle-Simpson Aquifer, South-Central Oklahoma. U.S.G.S. Geological Survey, v. Scientific Investigations Report 2011-50290, 121 pp.

Dalhberg, E.C. 1995. Applied hydrodynamic in petroleum exploration: Springer- Verlag, New York, 281 pp.

do Nascimento, A. F., Lunn, R. J., and Cowie, A. 2005 Numerical modelling of pore-pressure in a reservoir-induced seismicity site in northeast Brazil. Geophysics Journal International, 160, p. 249-262.

Domenico, P.A. and Schwartz, F.W. 1990. Physical and Chemical Hydrogeology, New York, John Wiley & Sons, 824 pp.

Domenico, P.A. and Mifflin, M.D. 1965. Water from low-permeability sediments and land subsidence, *Water Resources Research*, 1: 4, p. 178-186.

Ellsworth, W.L. 2013. Injection -induced earthquakes. *Science*, 341.

El-Dessouky, H.T., and Ettouney, H.M. 2002. Fundamentals of Sea Water Desalination. Amsterdam: Elsevier Science. 690 pp.

Fetter, C.W., 2001, Applied Hydrogeology 4th Ed.: New Jersey, Prentice Hall, 598 p.

Franseen, E.K., Byrnes, A.P., Cansler, J.R., Steinhauff, D.M., Carr, T.R., and Dubois, M.K. 2003. Geological Controls on Variable Character of Arbuckle Reservoirs in Kansas: An Emerging Picture. Kansas Geological Survey Open-file Report (2003-59), 30 pp.

Franseen, E. K., and Byrnes, A. P., 2012, Arbuckle Group platform strata in Kansas—A Synthesis; in, The Great American Carbonate Bank: The Geology and Economic Resources of the Cambrian–Ordovician Sauk Megasequence of Laurentia: AAPG Memoir 98, J. R. Derby, R. D. Fritz, S. Longacre, W. A. Morgan, and C. A. Sternbach, p. 1031–1047

Fritz, R.D., Medlock, P., Kuykendall, M.J., and Wilson, J.L. 2013. The geology of the Arbuckle Group in the Midcontinent; sequence stratigraphy, reservoir development, and the potential for hydrocarbon exploration. AAPG Search and Discovery Article #30266, 12 pp.

Goebel, T.H.W., Weingarten, M., Chen, X., Haffener, J., and Brodsky, E.E. 2017. 2016 Mw5.1 Fairview, Oklahoma earthquakes: Evidence for long-range poroelastic triggering at >40 km fluid disposal wells. *Earth and Planetary Science Letters*, 472, p. 50-61.

Harbaugh, A.W. 2005. MODFLOW-2005, The U.S. Geological Survey modular ground-water model—the ground-water flow process. U.S. Geological Survey Techniques and Methods 6-A16.

Hsieh, P.A., and Bredehoeft, J.D. 1981. A Reservoir Analysis of the Denver Earthquakes: A Case of Induced Seismicity. *Journal of Geophysical Research*, 86: B2, p. 903-920.

Hornbach, M.J., DeShon, H.R., Ellsworth, W.L., Stump, B.W., Hayward, C., Frohlich, C., Oldham, H.R., Olson., J.E., Magnani, M.B., Brokaw, C., and Luetgret, J.H. 2015. Causal factors for seismicity near Azle, Texas. *Nature Communications*, 6:6728.

Johnson, K.S. 1991. Geologic Setting of the Arbuckle Group in Oklahoma. Oklahoma Geological Survey Special Publication 91-3, pp. 12.

Johnson, K. S. 2008. Geologic History of Oklahoma. Oklahoma Geological Survey Educational Publication 9, 6 pp.

Keranen, K. M., Savage, H.M., Abers, G., and Cochran, E. 2013. Potentially induced earthquakes in Oklahoma, USA: Links between wastewater injection and the 2011 Mw 5.7 earthquake sequence. *Geology*, 41:6, p. 699-702.

Keranen, K. M., Weingarten, M., Abers, G.A., Bekins, B.A., and Ge, S. 2014. Sharp increase in central Oklahoma seismicity since 2008 induced by massive wastewater injection. *Science*, 345: 6195, p. 448-451.

Kroll, K. A., Cochran, E. S., and Murray, K. E. 2017. Poroelastic properties of the Arbuckle Group in Oklahoma derived from well fluid level response to the 3 September 2016 Mw 5.8 Pawnee and 7 November 2016 Mw5.0 Cushing Earthquakes. *Seismological Research Letters*, 22: 4, p. 963-970.

Marsh, S. and Holland, A. 2016. Comprehensive Fault Database and Interpretive Fault Map of Oklahoma. Oklahoma Geological Survey Open-File Report (OF2-2016), 15 pp.

McGarr, A., and Barbour, A.J. 2017. Wastewater disposal and the earthquake sequences during 2016 near Fairview, Pawnee, and Cushing, Oklahoma. *Geophysical Research Letters*, 44, p. 9330–9336.

Milad, B., and Slatt, R. 2017. Integrated 3-D Seismic, Outcrop, and Core Data for Characterization of Natural Fractures of the Hunton Limestone and the Woodford Shale in Central Oklahoma. Adapted from poster presentation. AAPG 2017 Annual Convention and Exhibition. Houston, TX. April 2-5, 2017.

Murray, K.E. 2015. Class II Saltwater Disposal for 2009–2014 at the Annual-, State-, and County- Scales by Geologic Zones of Completion, Oklahoma. Oklahoma Geological Survey Open-File Report (OF5-2015), 18 pp.

National Research Council. 2012. Induced seismicity potential in energy Technologies. National Academy of Sciences, Washington D.C., National Academies Press, 300 pp.

Northcutt, R. A., and Campbell, J. A. 1995. Geological provinces of Oklahoma. Oklahoma Geological Survey Open-File Report (OF5-95).

Ogwari, P.O., and Horton, S.P. 2016. Numerical model of pore-pressure diffusion associated with the initiation of the 2010-2011 Guy-Greenbrier, Arkansas earthquakes. *Geofluids*, 16, p. 954-970.

Perilla-Castillo, Paula. 2017. *Rock properties derived from analysis of earth tide strain observed in continuous pressure monitoring of the Arbuckle Group of Oklahoma* (Master's thesis). Retrieved from https://shareok.org/handle/11244/50808

Peterie, S.L., Miller, R.D., Intfen, J.W., and Gonzales, J.B. 2018. Earthquakes in Kansas Induced by Extremely Far-Field Pressure Diffusion. *Geophysical Research Letters*, 45, p. 1395-1401

Puckette, James. 1996. *Evaluation of underpressured reservoirs as potential repositories for liquid waste* (Doctoral dissertation). Access from ProQuest Dissertations and Theses. (UMI No. 9730453)

Puckette, J. and Al-Shaieb, Z. 2003. Naturally underpressured reservoirs: applying the compartment concept to the safe disposal of liquid waste: AAPG Search and Discovery Article #40071, 15 pp.

Puckette, J., Halihan, T., and Faith, J. 2009. Characterization of the Arbuckle-Simpson aquifer: Oklahoma Water Resources Board, Arbuckle-Simpson Aquifer Special Study, 53 pp.

Ragland, D. A., and Donovan, R. N. 1991. Sedimentology and Diagenesis of the Arbuckle Group in Outcrops of Southern Oklahoma: Oklahoma Geological Survey Special Publication, 91-3, 21 pp.

Reilly, T.E., and Harbaugh, A.W. 2004. Guidelines for Evaluating Ground-Water Flow Models. U.S. Geological Survey Scientific Investigations Report 2004-5038-Version 1.01.

Scheffer, A.A. 2012. *Geochemical and microbiological characterization of the Arbuckle Saline Aquifer, a potential CO2 storage reservoir; implications for hydraulic separation and caprock integrity* (Master's thesis). Retrieved from https://kuscholarworks.ku.edu.

Walsh, F.R., and Zoback, M.D. 2015. Oklahoma's Recent earthquakes and salt water disposal. *Science Advances*, 1: 5.

Weingarten, M., Ge, S., Godt, J.W., Bekins, B.A., and Rubinstein, J.L. 2015. High-rate injection associated with the increase in U.S. mid-continent seismicity. *Science*, 348: 6241, p. 1336-1340.

Williams, Jordan. 2017. *Geologic, Permeability, and Fracture Characterization of the Arbuckle Group in the Cherokee Platform, Oklahoma* (Master's thesis). Retrieved from https://esirc.emporia.edu/bitstream/handle/123456789/3562/Jordan%20Williams.pdf?sequence=1

Zhang, Y., Person, M., Rupp, J., Ellett, K., Celia, M.A., Gable, C.W., Bowen, B., Evans, J., Bandilla, K., Mosley, P., Dewers, T., and Elliot, T. 2013. Hydrogeologic Controls on Induced Seismicity in Crystalline Basement Rocks Due to Fluid Injection into Basal Reservoirs. *Groundwater*, 51: 44, p. 525-538.

Wang, H. F., and Anderson, M.P. 1982. Introduction to Groundwater Modeling: Finite Difference and Finite Element Methods. San Diego, Academic Press, Inc., 237 pp.

Yeck, W.L. Weingarten, H.M., Benz, H.M., McNamara, D.E., Bergman, E.A., Herrmann, R.B., Rubinstein, J.L., and Earle, P.S. 2016. Far-field pressurization likely caused one of the

largest injection induced earthquakes by reactivating a large preexisting basement faults structure. *Geophysics Research Letters*, 43, p. 10193-10207.

Appendix A: Sensitivity Analysis Plots for Transient Model

